JOURNAL OF GEOPHYSICAL RESEARCH, VOL. 106, NO. B2, PAGES 1987–2003, FEBRUARY 10, 2001

Transition from circular to stellate forms of submarine volcanoes

Neil C. Mitchell[1]

Department of Earth Sciences, University of Oxford, Oxford, England, United Kingdom

Abstract. Large volcanic islands and guyots have stellate forms that reflect the relief of radiating volcanic rift zones, multiple volcanic centers, and embayments due to giant flank failures. Small mid-ocean ridge volcanoes, in contrast, are commonly subcircular in plan view and show only embryonic rift zones. In order to characterize the transition between these two end-members the morphology of 141 seamounts and guyots was studied using the shape of the depth contour at half the height of each edifice. Irregularity was characterized by measuring perimeter distance, elongation, and moment of inertia of the contours, assuming an "ideal" edifice is circular. The analysis reveals a general transition over 2-4 km edifice height (best transition estimate 3 km), while some large edifices 4-5 km high show no major embayments or ridges, suggesting considerable variation in the effectiveness of mechanisms that cause flank instability and growth of rift zones. The various origins of the transition are discussed, and the upper limit of magma chambers, many of which lie above the basement of the larger edifices, is proposed to affect the morphologic complexity via a number of mechanisms and is an important factor affecting the mode of growth. The origins of the truncated cone shape of mid-ocean ridge volcanoes are also discussed. Of the eruption mechanisms that have been proposed to explain their flat summits, the most likely mechanisms involve eruption from small ephemeral magma bodies lying within the low-density upper oceanic crust. The discussion includes speculations on factors affecting the depths of magma chambers beneath oceanic volcanoes.

1. Introduction

Small mid-ocean ridge volcanoes are simple round truncated cones with collapse pits, craters, or calderas in their summits [*Hollister et al.*, 1978]. Large seamounts, guyots, and volcanic ocean islands have more complex shapes, however, showing multiple volcanic centers, radiating ridges interpreted as volcanic rift zones, and embayments associated with lobes deeper in seamount flanks believed to represent debris avalanches [*Vogt and Smoot*, 1984]. The mid-ocean ridge volcanoes in Figure 1 and El Hierro of the Canary Islands in Figure 2 illustrate these two morphological extremes. While mid-ocean ridge volcanoes show a variety of forms [*Batiza and Vanko*, 1983], they are clearly simpler features compared to El Hierro island. *Vogt and Smoot* [1984] noticed this transition in the Geisha Guyots and proposed that the variation from small round volcanoes to large stellate guyots represented edifices where volcanic activity had terminated at different stages, with large edifices having progressively developed rift zones and archipelagic aprons of debris with associated collapse structures. *Binard et al.* [1992] described young seamounts of the southeast end of the Society and Austral volcanic island chains, which show incipient rift zones on 1800 m high edifices and well-developed rift zones on 3700-4000 m high edifices, though no clear evidence for flank collapses.

With the accumulation of multibeam sonar data from mid-ocean ridges and new data on large oceanic islands such as El Hierro revealing details of landslides and other erosional and volcanic features, it is timely to reexamine this transition. In the following, the edifice height over which the morphologic transition occurs is quantified, and the factors that contribute to the stellate form are discussed in the light of the transition height value and current ideas on the development of rift zones and flank collapse. The dominant cause of the morphologic transition is proposed to be the upper limit of magma chambers within edifices, with some small volcanoes having shallow ephemeral magma chambers within their basement and with many tall volcanoes having magma chambers above their basement. The term "seamount" is loosely used to refer to all submarine volcanic edifices regardless of size.

2. Seamount Selection

Seamount midheight contours are shown in Figure 3, arranged in order of edifice height and with their scales normalized so that the shapes of small and large edifices can be compared. Figure 4 shows their locations. Seamounts were selected according to whether they appeared to be isolated volcanic structures, avoiding those obviously affected by later faulting or where summit calderas breached edifice walls. The selection is inevitably imperfect as the small seamounts are created during short-lived volcanic events, whereas large edifices grow over longer periods often with multiple volcanic centers [*Batiza and Vanko*, 1983]. Many of these seamounts were created in chains above mantle melting anomalies, so relatively isolated edifices were selected to avoid volcanoes that were coalesced along the chain. The following analysis shows that elongations (aspect ratios) of the large and small edifices are not significantly different so the selection was at least consistent in this respect. For some features a contour slightly above the midheight provided a better representation of the shape of the main volcano. For example, a satellite volcano in seamount 137 (Figure 3) was excluded by

[1]Now at Department of Earth Sciences, Cardiff University, Cardiff, Wales, United Kingdom

Paper number 2000JB900263.
0148-0227/01/2000JB900263$09.00

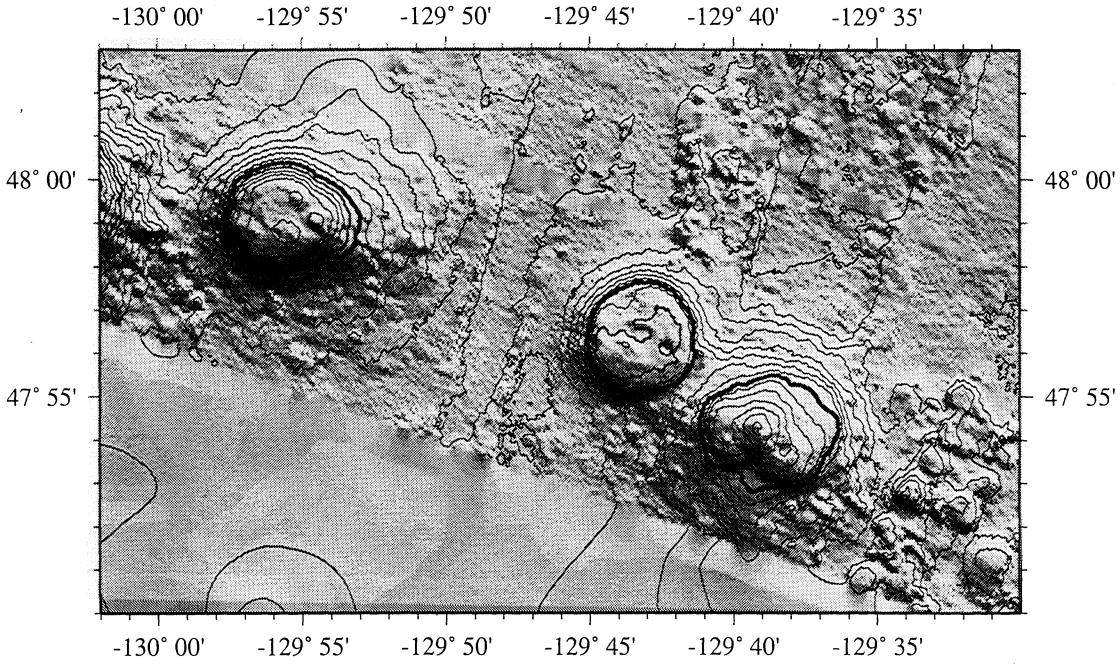

Figure 1. A small chain of mid-ocean ridge volcanoes (data from a multibeam synthesis [*Keeley et al.*, 1994]). Contours are every 100 m. The midheight contours are darkest. Note that the westerly volcano has a slight east-southeast protrusion and the far easterly volcano may consist of two volcanic centers, but otherwise they are relatively circular structures.

choosing a higher contour level (138). The following characteristics are shown for both the midheight contours and the alternate contours.

Heights were measured directly from contour maps to the base of each structure, a procedure that ignores sediment ponded around the base (biasing heights by mostly <500 m based on regional seismic data [*Ewing et al.*, 1968]). Heights may be overestimated for northcentral Pacific guyots because of thick summit carbonate caps [*Winterer et al.*, 1995], but guyots are taller than the height transition so overestimation will not affect the resolved transition value. Height estimates also ignore effects of edifice subsidence due to loading, although this should also affect only the largest edifices. The following graphs give the heights of guyots adjusted for erosion by using the correlation between elevation and area for modern volcanic islands [*Vogt and Smoot*, 1984]. The regression in Figure 5 was used to predict original island elevations (horizontal shaded band) from guyot summit areas (crosses), assuming that the majority of these guyot tops are erosional features rather than carbonate platforms [*Winterer et al.*, 1995]. From the data dispersion in Figure 5, the adjustment uncertainty is generally <1000 m.

The contours of small seamounts were mostly extracted from gridded multibeam echo sounder data from mid-ocean ridges. These include ridges off the west coast of the United States [*Keeley et al.*, 1994], northern and southern East Pacific Rise [*Macdonald et al.*, 1992; *Scheirer et al.*, 1996], and three Cretaceous seamounts near Hawaii [*Moore and Chadwick*, 1995] (National Ocean Service data from the National Geophysical Data Center). Data spatial resolution is nominally 100, 300, 200, and 200 m for the *Keeley et al.* [1994], *Macdonald et al.* [1992], *Scheirer et al.* [1996], and National Ocean Service data sets, respectively. Actual resolution of the *Macdonald et al.* [1992] data set is coarser than 200 m because it includes lower-resolution sonar data, but there is no substantial anomaly in their shape characteristics. The El Hierro multibeam data (Figure 2) were filtered and resampled to 1500 m resolution so that the extracted 1300 m contour (H in Figure 3) had a similar level of detail to the other data sets.

Contours were digitized from the sources given in the accompanying electronic supporting material[1]. The source charts are of varied quality, and some had been hand-drafted or had incomplete multibeam coverage, but the qualitative detail of these contours appears similar to that of contours extracted from digital data. The number of nodes representing each contour (Figure 6b), a measure of proportional resolution, is similar for both short and tall edifices. The contour level for guyots was taken at half the estimated original height before erosion.

Figure 3 shows the expected progression [*Vogt and Smoot*, 1984] from almost circular small mid-ocean ridge volcanoes to irregular large seamounts and guyots. Figure 3 also shows considerable variation, however. Some small volcanoes are significantly irregular, such as 19, 42, and 43. Contours 116 and 124 show promontories of radiating rift zones (edifices near Lowrie guyot [*Smoot*, 1989]) and 124 shows a landslide embayment on its north side (Makarov guyot [*Vogt and Smoot*, 1984]), but some contours of tall edifices are nearly circular, and their source maps can show a lack of obvious rift zones or landslides, for example, contours 125 and 143.

3. Characterizing Irregularity

Assuming an ideal seamount is circular, three dimensionless shape characteristics were calculated [*Mitchell*, 1998]. Each

[1]Supporting table is available via Web browser or via Anonymous FTP from ftp://kosmos.agu.org, directory "apend" (Username = "anonymous", Password = "guest"); subdirectories in the ftp site are arranged by paper number. Information on searching and submitting electronic supplements is found at http://www.agu.org/pubs/esupp_about.html.

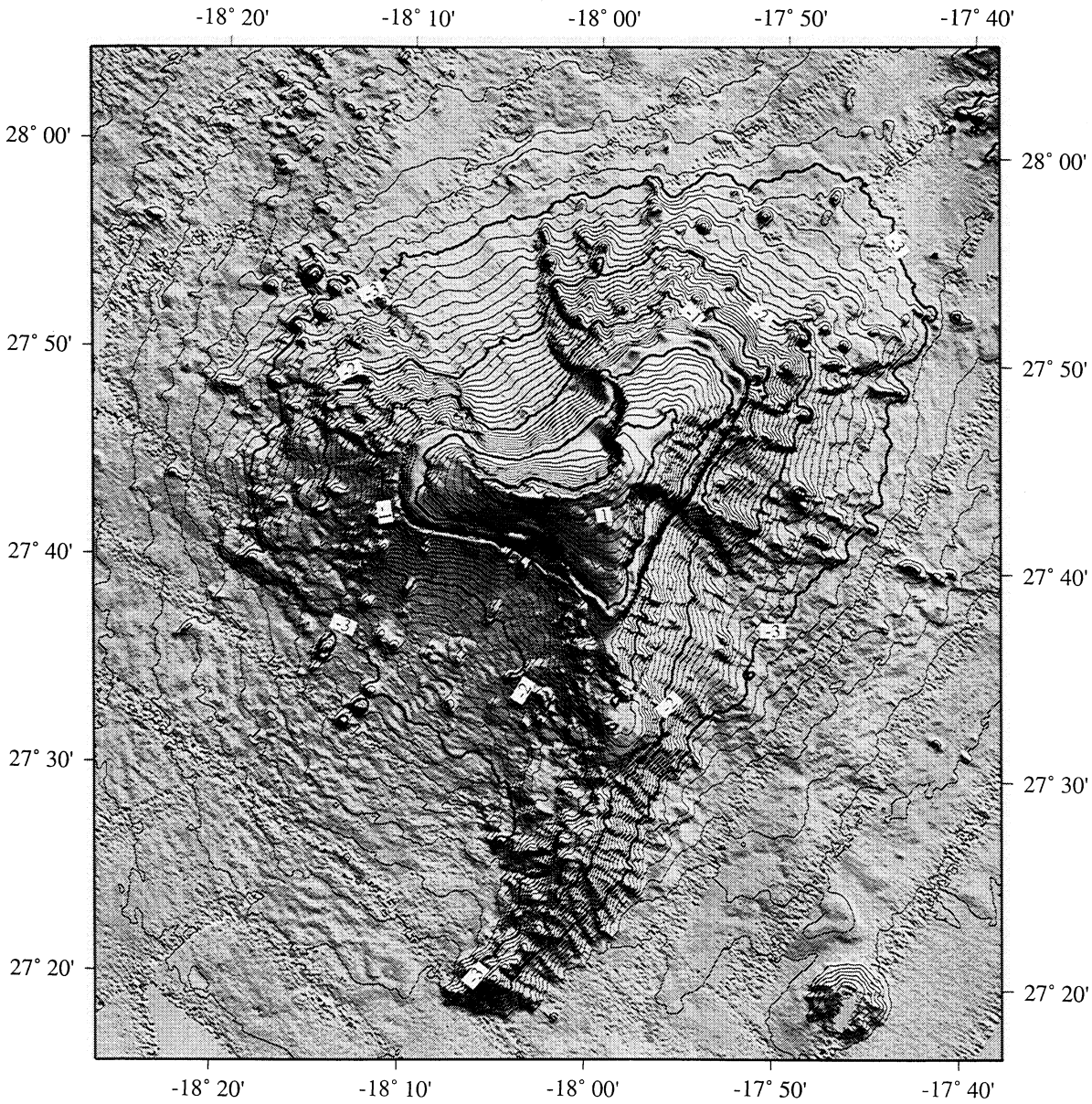

Figure 2. Multibeam bathymetry for El Hierro island of the Canaries [*Masson et al.*, 1998] showing embayments due to landslides and radiating volcanic ridges [*Carracedo*, 1994; *Gee*, 1999]. Multibeam bathymetry extends to within a few hundred meters of sea level, and intervening areas are interpolated. (Data are courtesy of D.G. Masson of the Southampton Oceanography Centre, England.)

contour in Figure 3 is represented by a series of nodes forming a closed polygon. Perimeter distance, defined as the sum of distances between the nodes (r_i), normalized by dividing by the circumference of a circle with the same area, was calculated from each polygon (units are omitted since the characteristics are dimensionless):

$$P = \frac{\sum_i r_i}{2\pi a}, \quad (1)$$

where $a = \sqrt{A/\pi}$ and A is the area of the polygon.

Elongation (aspect ratio) was calculated from the ratio of length scales required to subdivide each polygon by area in two orthogonal directions as follows (Figure 7). The contour was first used to generate a gridded version of its shape with grid values set to 1 inside the polygon and 0 outside. The grid was searched for the center of mass ("o" in Figure 7) by finding two orthogonal lines that each bisect the polygon by area, and locating their intersection. The direction of elongation was found by searching for a line through "o" which has the minimum sum of distances to all grid points within the polygon. The elongation line (through c-d in Figure 7) divides the area in two. The two halves of the polygon were further bisected by area to give points a and b in Figure 7, and similarly, c and d were found by bisecting areas in the orthogonal direction. Elongation (e) was then calculated from the ratio cd/ab.

Moment of inertia (MOI) was calculated about the center of mass. Each polygon was represented by a thin plate and its MOI

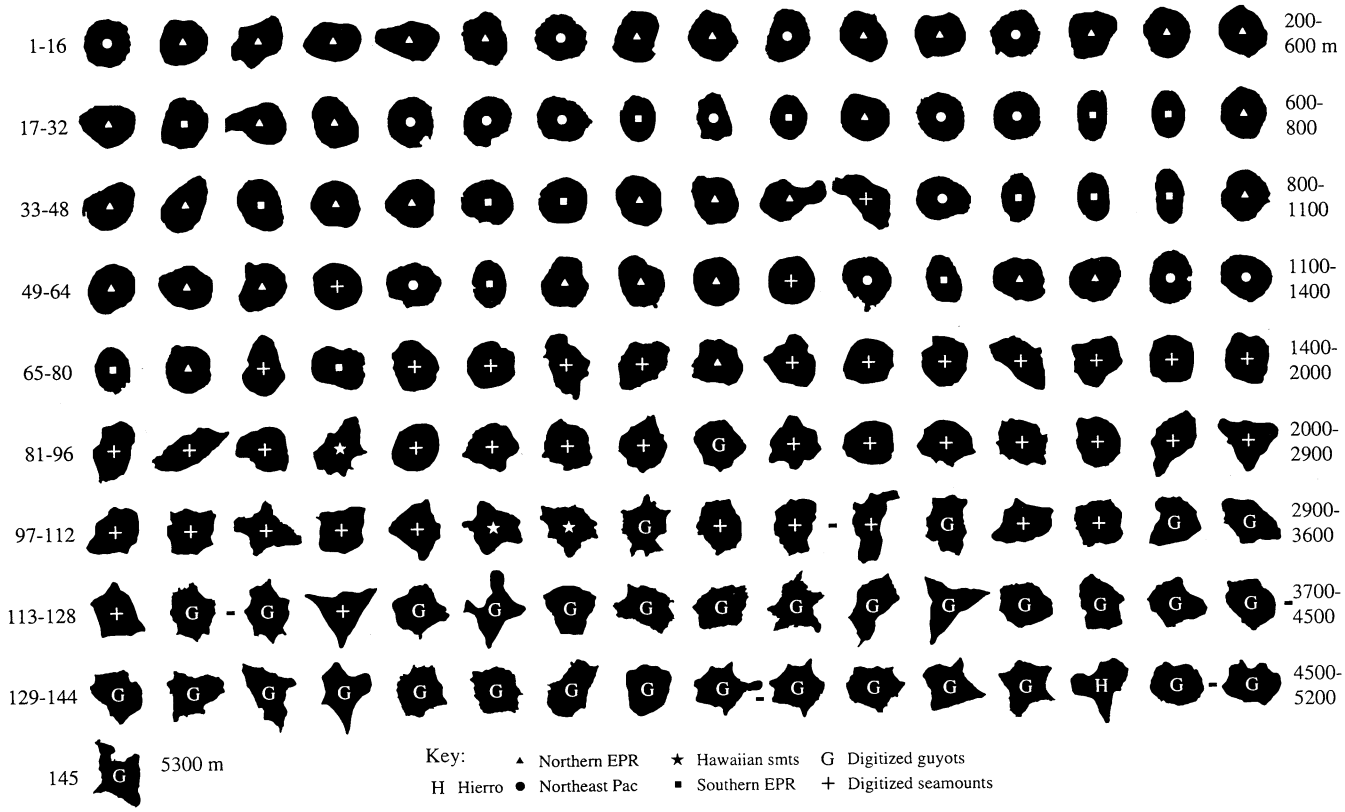

Figure 3. Compilation of midheight contours of seamounts arranged in order of increasing full height (given to the right of each row) and shown with scales normalized by dividing their dimensions by square root of area so that shapes of small and large seamounts can be compared. Legend in the key refers to data from El Hierro [*Masson et al.*, 1998], northern East Pacific Rise (EPR) [*Macdonald et al.*, 1992], northeast Pacific [*Keeley et al.*, 1994], near Hawaii [*Herlihy et al.*, 1988], and southern EPR [*Scheirer et al.*, 1996]. Sources of digitized guyots and seamounts are given in the electronic supporting material for this paper. Heights of guyots are adjusted for erosion. Where edifice contours were digitized at two different heights, the two contours are associated by a dash. Note the generally increasing irregularity down the figure, reflecting growth of volcanic rift zones and embayments due to landsliding but also increasing variability of forms.

divided by the MOI of a circular disc with the same area:

$$I = \frac{\Delta^2 \sum_i d_i}{0.5\pi a^4} - 0.5\left(e + \frac{1}{e}\right) + 0.1, \qquad (2)$$

where Δ is the grid cell spacing and d_i are the distances from "o" to each grid cell. MOI is strongly correlated with elongation [*Mitchell*, 1998] so the second term in (2), which is the MOI of an ellipse with elongation e, was subtracted to produce a more independent characteristic for the following graphs. The final constant (0.1) was added to ensure that the results are positive and to allow plotting with logarithmic scales. MOI is potentially useful because it is sensitive to the distribution of area away from the center. Star-shaped polygons, with promontories due to radiating flank rift zones, may have little elongation and moderate perimeter distance depending on the detail of the contour but should have large MOI owing to the widely spread promontories. MOI is also preferred because it is less sensitive to digitizing accuracy than perimeter distance.

To illustrate their application, perimeter distance, elongation, and MOI were calculated for each 100 m closed contour of El Hierro island, and Figure 8 shows these characteristics plotted versus contour height. Figure 2 shows an embayment on El Hierro's north side caused by the El Golfo debris avalanche [*Masson*, 1996], and further embayments along its southwest and southeast sides also reflect flank collapses [*Carracedo*, 1994; *Gee*, 1999]. The northeast, west, and south promontories of the island represent a "Mercedes" star of rift zones [*Carracedo*, 1994]. MOI reflects the general varied shape of contours with height; for example, large MOI at 1 km depth (-1 km in Figure 8) reflects the embayments and promontories between them. MOI decreases with depth to 3 km because the depositional aprons of debris avalanches create convex contours across embayments and hence a more nearly circular outline. Perimeter distance shows no systematic variation because changes in shape are compensated by increasing numbers of contour nodes, and hence contour detail, with depth. The gradual variation in both characteristics at 1 km depth means that the exact choice of contour level is not important, although contours slightly above midheight are preferable for representing landslide embayments.

4. Results

Perimeter distance is shown in Figure 6a (top), with both directly measured and extrapolated heights for guyots shown connected by dashed lines. Vertical solid lines connect values derived from alternative contours of the same seamount (i.e., contours in Figure 3 connected by dashes). Figure 6a (bottom)

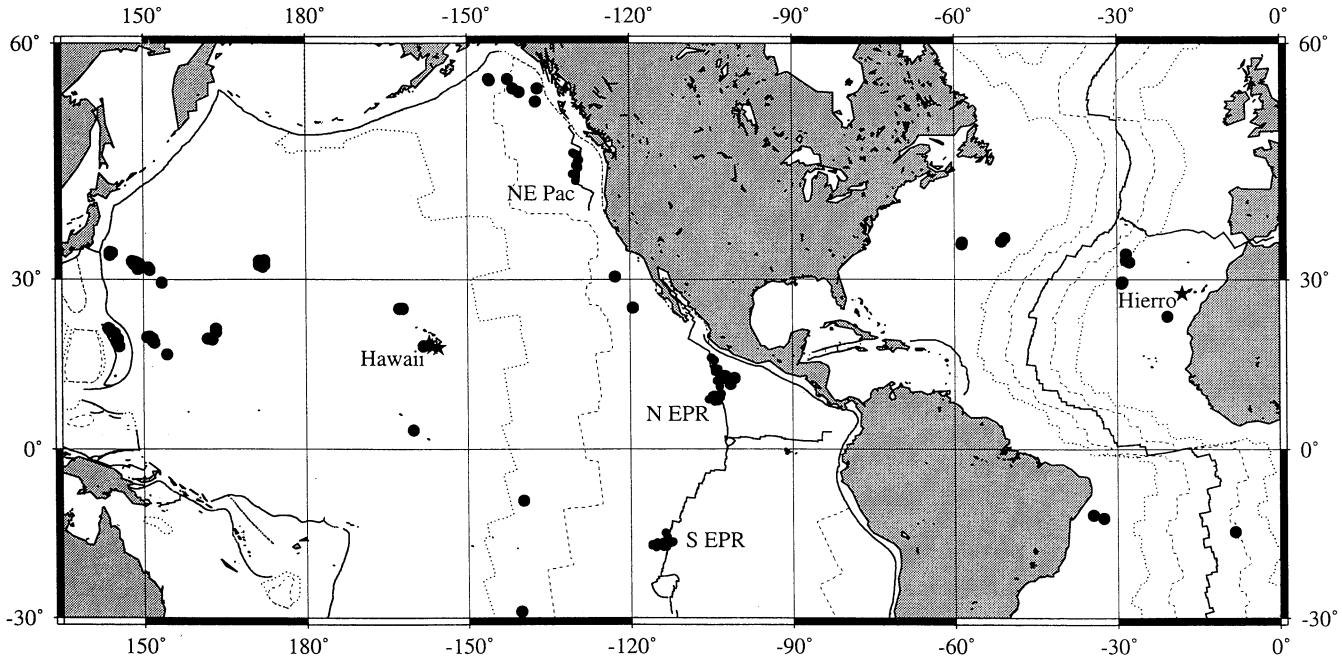

Figure 4. Locations of seamounts in Figure 3. Clusters marked NE Pac, N EPR, S EPR Hawaii, and Hierro mark data taken from digital data sets (annotation representing northeast Pacific, northern East Pacific Rise, southern East Pacific Rise, and data from near the Hawaiian islands and El Hierro, respectively). All other seamounts were digitized from published maps. Solid, dashed and dotted lines represent plate boundaries and 30 and 60 Ma isochrons, respectively [*Muller et al.*, 1997].

shows average perimeter distance calculated within 1 km height bins (solid circles) and 2 km height bins (large open circles) using the extrapolated guyot heights. Perimeter distance might be expected to increase with edifice size simply because assuming that midheight contours are fractal-like, the sonar will resolve increasingly better detail. However, because of the coarse nature of the published charts and contours digitized from them, the number of contour nodes for large edifices is similar to those for small edifices (Figure 6b) so the change in perimeter distance here is not an artifact. Figure 6c shows no resolvable change in mean elongation across the whole range, showing that seamounts were selected with uniform average aspect ratio. Figure 6 shows a general transition between 2 and 4 km for mean MOI. A confidence test applied to perimeter distance and MOI shows that the 0-2 km group is statistically different at the 95% level from the 2-4 km and 4-6 km groups, while the 2-4 km and 4-6 km groups are indistinguishable at 95%.

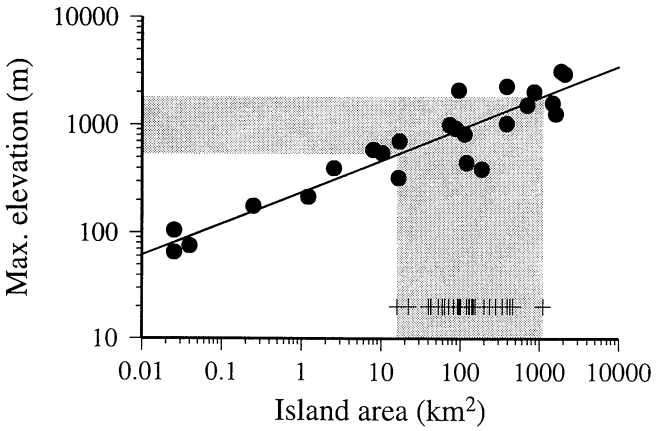

Figure 5. Maximum elevations of volcanic ocean islands [*Vogt and Smoot*, 1984] which are used to adjust guyot heights for subaerial erosion. The straight line is a logarithmic least squares regression. Crosses show the range of guyot summit areas, and shading shows the range of inferred elevations using the regression.

The best estimate of the transition height is defined here as the height corresponding to half the total change in a characteristic using the 0-1 km and 4-6 km averages as end-members. Using the characteristics averaged in 1-km bins as the dependent variable, transition heights are 2.8 and 3.0 km for perimeter distance and MOI, respectively. As a conservative measure of the uncertainty range, a 2-km running mean was computed, and the uncertainty range is defined as that where the running mean was within 2σ of the transition value, accounting also for uncertainty in the transition value. The transition heights and uncertainties are therefore 2.8 (1.6-∞) and 3.0 (2.0-∞) km for perimeter distance and MOI, respectively, where the upper uncertainty limits are undefined because of data variability. Considering also the ~500 m uncertainty in measuring edifice heights, the transition occurs at a minimum height of 1.5 km for MOI. The data set is too small to show the structure of the transition, but Figures 6a and 6d are more consistent with a gradual than with an abrupt transition. Furthermore, while large seamounts are on average more irregular than small seamounts, the variability of forms is also greater, such that near-circular forms of some large seamounts lead to small irregularity characteristics.

For comparison with the transition in Figure 6, Figure 9 shows the lengths of rift zones. Short rift zones in small edifices are difficult to interpret from bathymetry alone, and ridges left by adjacent flank failures could be mistaken for rift zones. Nevertheless, linear features are interpretable on edifices higher than 2000 m and become dramatically longer where the edifice height was >5000 m, a feature attributed [*Vogt and Smoot*, 1984] to efficient transport of low-viscosity magma down rift zones.

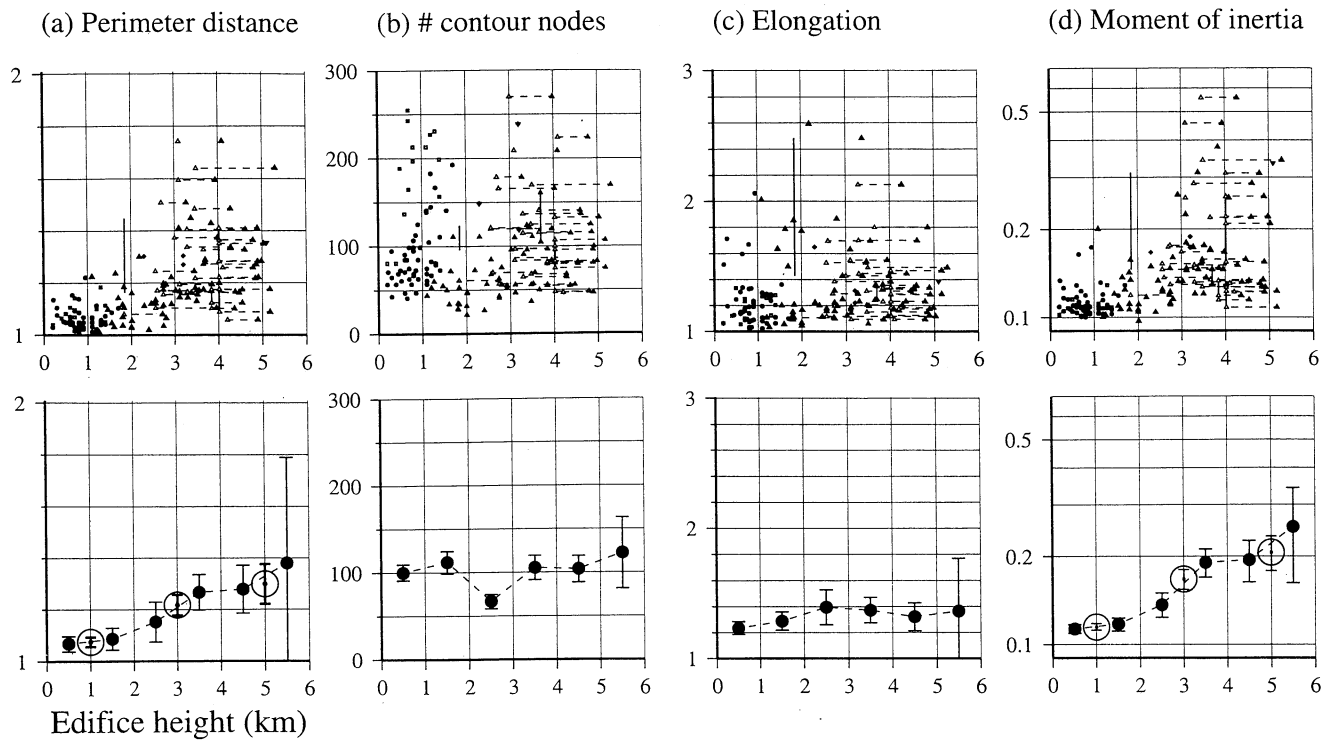

Figure 6. Characteristics of the midheight contours in Figure 3 shown versus total edifice height. (top) Dashed lines connect heights of guyots taken directly from charts and their heights adjusted for subaerial erosion. Symbols represent characteristics of hand-digitized contours (triangles) and contoured digital data from northern and southern EPR (solid circles), northeast Pacific ridges (open squares), near Hawaii (solid diamonds), and El Hierro island (inverted triangle). Vertical solid lines connect measurements for the alternative contours associated by dashes in Figure 3. (bottom) The characteristics averaged in 1-km and 2-km bins are shown (error bars are 1σ). Perimeter distance and moment of inertia show a transition over 2-4 km edifice height.

Binard et al. [1992] interpreted rift zones from bathymetry of two seamounts in the Society chain that were shallower than 2000 m, but otherwise the general lack of major ridges interpretable as rift zones in edifices smaller than 2000 m [*Batiza and Vanko*, 1983] supports the idea that there is a fundamental change in the way volcanoes grow above 2000 m.

5. Discussion

The question of why there is a change to stellate volcano forms with volcano height prompts the question as to why small mid-ocean ridge volcanoes are circular, so this is addressed first. Likely explanations imply that they are fed from small ephemeral magma bodies within the upper oceanic crust. The origin and transition to the stellate form are then addressed. The discussion develops the following interpretation for seamount growth (Figure 10). Small mid-ocean ridge seamounts grow with magma bodies within their basement (at the brittle-ductile transition [*Smith and Cann*, 1992] or at shallow density-trapping or freezing levels). The horizon of neutral buoyancy lies close to the seafloor initially [*Hooft and Detrick*, 1993] so intrusion can create shallow laccoliths and sills [*Lonsdale*, 1983; *Staudigel and Schminke*, 1984], and eruption from cone sheets and other mechanisms can create flat-topped volcanoes. With further growth, magma bodies continue to lie within their basement until the seamount reaches 2-4 km height at which point some magma bodies can lie above edifice basement, leading to morphologically more complex stellate volcanoes because of more efficient supply of magma to rift zones and other processes.

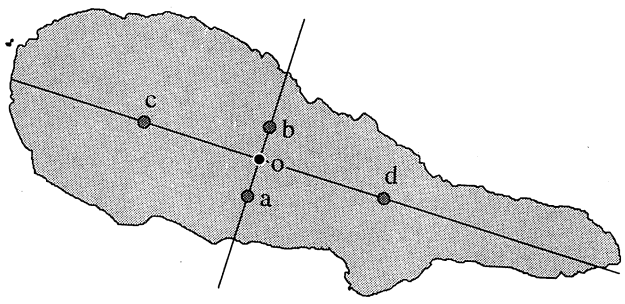

Figure 7. Illustration of how the direction of elongation and aspect ratio of the contours are calculated (example shown is the coastline of Pico island of the Azores). The letter "o" is the polygon's center of mass, and points a, b, c, and d (area bisectors along the lines shown) are used to calculate the polygon's elongation or aspect ratio.

5.1. Origin of the Flat-Top Form of Mid-ocean Ridge Volcanoes

The processes involved in growth of mid-ocean ridge volcanoes have been addressed by many authors from submersible field observations, sampling, and sonar data and by comparison with volcanoes in the Galapagos islands and central volcanoes on Iceland, which are arguably the closest subaerial analogues of mid-ocean ridge volcanoes. Various arguments suggest that magma chambers beneath these volcanoes, where they exist, are probably shallow.

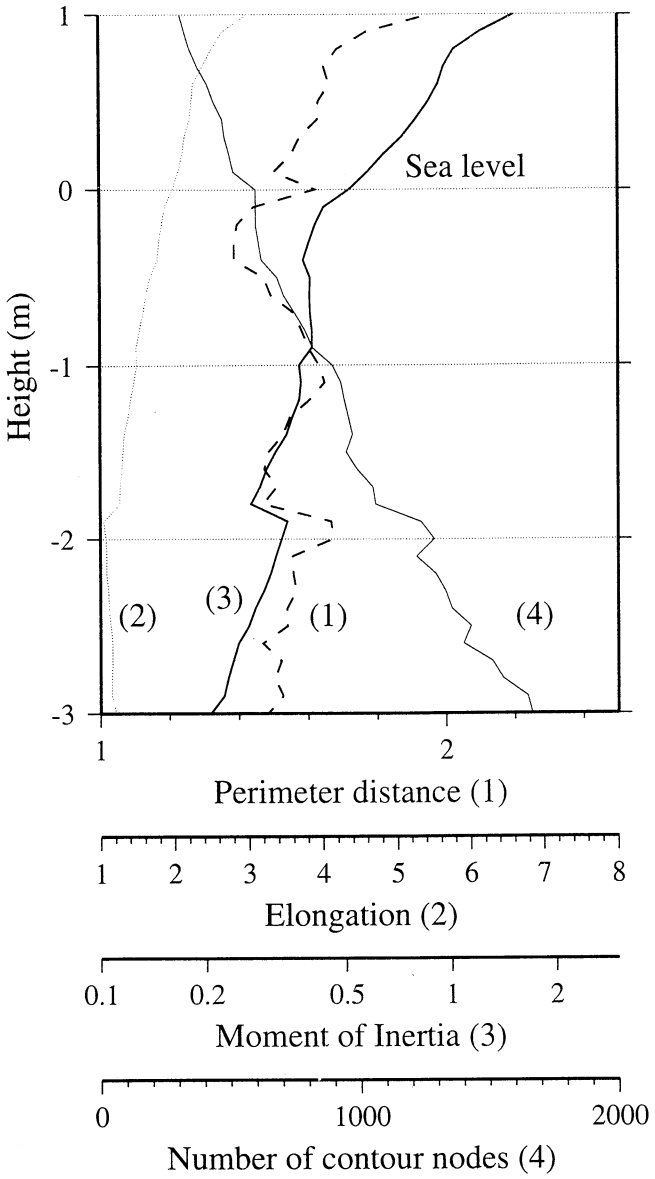

Figure 8. Characteristics calculated for the innermost closed contour of El Hierro island (Figure 2). The gradual variation in perimeter distance and moment of inertia (MOI) at around -1 km, the midheight of the edifice, implies that the exact choice of contour level is unimportant for representing edifice shape. Contours deeper than -1 km have smaller MOI than higher contours because depositional aprons of debris avalanches smooth contours across embayments, leading to more nearly circular contours.

5.1.1. Eruptive ring dike or cone sheet model. To explain flat-topped oceanic volcanoes, *Batiza and Vanko* [1983] preferred the explanation of *Simkin* [1972] for Galapagos volcanoes in which eruptions from ring dikes progressively fill the encircled region because of its small area compared to the volcano flanks, leading to a flat summit. *McBirney and Williams* [1969] also attributed the steep upper slopes of Galapagos volcanoes to lateral distension by ring dike intrusions. Possible eruptive circumferential ring fractures on seamounts have been observed with sonar and submersible [*Batiza et al.*, 1984, 1989; *Lonsdale and Spiess*, 1979]. Figure 11 compares the slopes of an oceanic volcano with those of three Galapagos volcanoes and shows that differences can mostly be attributed to the difference between subaerial and submarine lava eruption.

Some evidence suggests that cone sheets rather than ring dikes are involved. *Walker* [1984] noted that vent rings in some subaerial volcanoes lie outside central calderas and are more consistent with their being fed by cone sheets than by vertical ring dikes. Circular volcanic ridges and summit benches [*Batiza et al.*, 1989; *Batiza and Vanko*, 1983] are likely submarine equivalents of subaerial vent rings and they also occur outside collapse calderas, suggesting a different origin, as also supported by the observation that lava erupted at rapid rates in summit benches predate caldera collapse [*Batiza et al.*, 1989]. *Eddy et al.* [1998] interpreted a 200-m-high mound of pillow lava in the Troodos ophiolite on Cyprus as a small seamount fed from a shallow magma body. The edifice shows inward dipping sheets which are cut by outward dipping dikes and near-vertical faults, a sequence they attributed to cone sheet intrusion during eruption followed by collapse associated with caldera formation. Eroded central volcanoes on Iceland also commonly reveal massive complexes of centrally inclined sheets [*Gautneb and Gudmundsson*, 1992; *Gautneb et al.*, 1989; *Gudmundsson*, 1998b]. Modeling of Galapagos volcano stresses [*Chadwick and Dieterich*, 1995] suggests that circumferential dikes are probably not vertical but inclined. Furthermore, the interpretation of hyaloclastites on summits as caused by lava fountaining [*Batiza et al.*, 1984; *Smith and Batiza*, 1989] implies magma overpressure as required for cone sheet intrusion.

To explore the eruption geometry and likely depths of the sources of cone sheets, Figure 12 shows the orientations of maximum compressive stress in *Gudmundsson's* [1998b] model for elastic deformation around overpressured shallow magma chambers beneath Icelandic central volcanoes. The points on the chamber wall where rupture is most likely to occur (solid circles in Figure 12) have maximum compressive stress axes oriented 45° from the vertical, which correspond to the average dip of sheets in field mapping [*Gautneb and Gudmundsson*, 1992]. Sheets are predicted to intrude parallel to maximum compressive stress, to be steeply dipping above the chamber and shallower dipping to the sides, as observed in the field mapping, and to curve becoming steeper toward the free upper surface. The model is clearly simplistic, ignoring chamber geometry, loading by the volcano, and any regional (tectonic) loading, but it suggests a rough correspondence between the width of the area of eruption and the depth of the chamber. For the sake of argument, if the most common dip of sheets is 45° (corresponding to the stress minima at the chamber walls in Figure 12) and if it is assumed that they are the outermost sheets most likely to erupt around the summit margins, the summit diameters of flat-topped seamounts correspond to chamber depths as shown in Figure 13a. Figure 13b shows source depths (right coordinate scale) calculated from the summit diameters assuming an outer eruptive sheet dip angle θ of 45° (the average dip observed in Icelandic central volcanoes [*Gautneb and Gudmundsson*, 1992], the British Tertiary Province [*Richey*, 1961], and Gran Canaria cone sheets [*Schirnick et al.*, 1999]). Considering that Figure 13a ignores the finite width of the magma chamber and that arcuate summit benches could be the main locus of eruption [*Batiza et al.*, 1989] rather than the summit edges, this geometry will overestimate chamber depths, while ignoring sheet curvature will underestimate their depths. The dips of eruptive cone sheets are speculative in this model, but it can probably be inferred that most sources lie within the upper oceanic crust ($Z<2$ km in Figure 13b) rather than several kilometers deep in the lower oceanic crust.

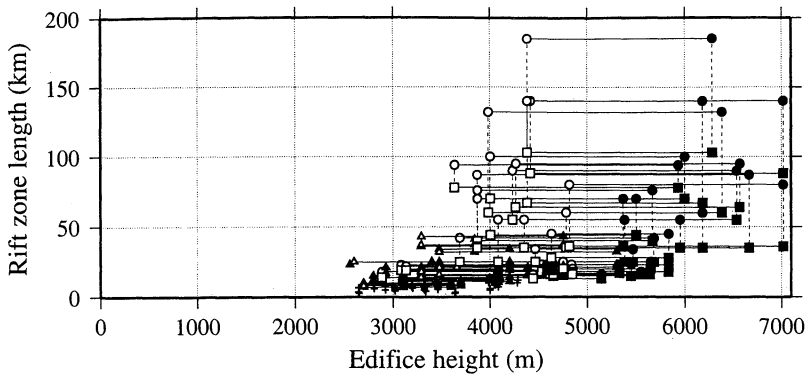

Figure 9. Rift zone lengths of some edifices studied here (triangles) and from *Vogt and Smoot* [1984] (other symbols). Open symbols show data where edifice heights were measured directly, while solid symbols represent heights of guyots extrapolated to account for subaerial erosion. For the *Vogt and Smoot* [1984] data, heights were also adjusted for sediment thickness. Circles and squares associated by dashed lines show maximum and average lengths for each edifice. Crosses show individual lengths for small edifices. *Vogt and Smoot* [1984] mention that no rift zones were interpretable below 2000 m edifice height. Rift zones only above 2500 m and rapidly increasing lengths for edifices originally taller than 5000 m are shown

The truncated cone form (Figure 11a) could therefore be explained simply if magma rising from depth sometimes stalls in the upper oceanic crust where it encounters extrusive rock of low density and temperature and intrudes small ephemeral laccoliths. As the laccoliths inflate, they extend the overlying crust and feed cone sheets with a range of dips, though with the dominant eruptive sheet corresponding to the preferred intrusion dip of 45°. Arcuate summit benches [*Batiza and Vanko*, 1983] may reflect irregular magma transport up cone sheets, while the steep outer talus slope (~30°) reflects the disintegration of material from the outer edge created by the outermost eruptive cone sheets. The outer slope could also be steepened by noneruptive cone sheets intruded below the outermost eruptive sheet as suggested for Galapagos volcanoes [*Williams and McBirney*, 1979], and dilation above noneruptive cone sheets could be the cause of the circumferential fractures. The variable flatness of mid-ocean ridge volcanoes [*Smith*, 1996] could merely reflect variable laccolith depth, with deep laccoliths leading to flat volcanoes, while sharp cones occur where magma has erupted directly without stalling in the extrusive layer. Sagging or collapse associated with satellite eruptions, intrusions or magma contraction on cooling or degassing can later produce summit calderas, craters, and collapse pits [*Batiza et al.*, 1984; *Fornari et al.*, 1984; *Smith and Batiza*, 1989], so cone sheet intrusion and collapse structures are not necessarily incompatible. If gas drive is relatively unimportant in deep water eruptions, a possible objection to the cone sheet model is that shallow (<1 km depth) magma bodies may not have sufficient overpressure from lithostatic loading to erupt because overlying extrusive rocks have lower mean density than the magma [*Smith and Cann*, 1992]. However, initial inflation of the laccolith would probably lead to intrusions into the overlying carapace which rapidly solidify to raise the density of the lid sufficiently to allow eruption [*Lonsdale*, 1983]. *Bryan et al.* [1994] interpreted some short (<100 m high) flat-topped edifices as megatumuli (inflated crusts of surface lava deltas or lakes), an analogous explanation to the one here, although their structures represent more superficial inflation.

Caldera dimensions provide clues to magma chamber geometry. The open circles in Figure 14 show diameters of calderas and craters observed in multibeam and side-scan sonar data sets [*Barone and Ryan*, 1990; *Cochran et al.*, 1993; *Scheirer et al.*, 1996] which were supplemented with other published

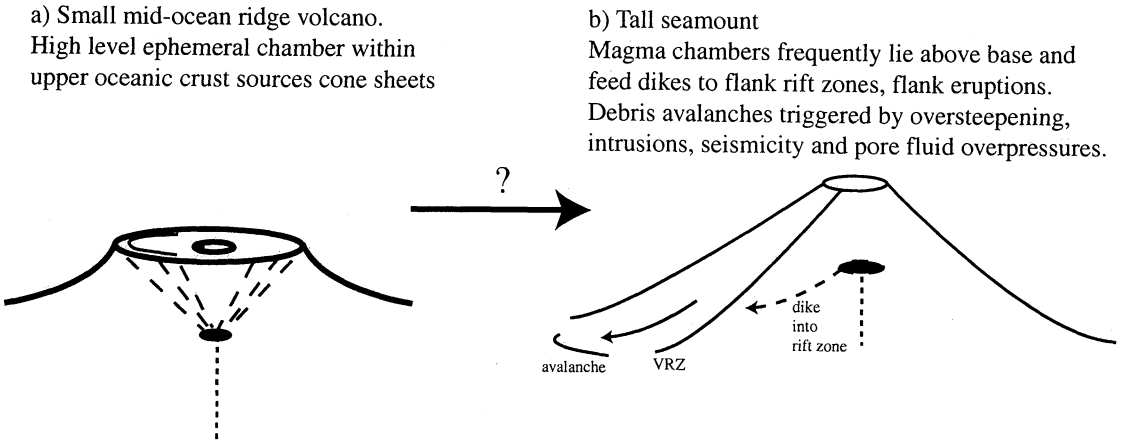

Figure 10. Summary of the speculative origins of the two morphological end-members. VRZ represents volcanic rift zone.

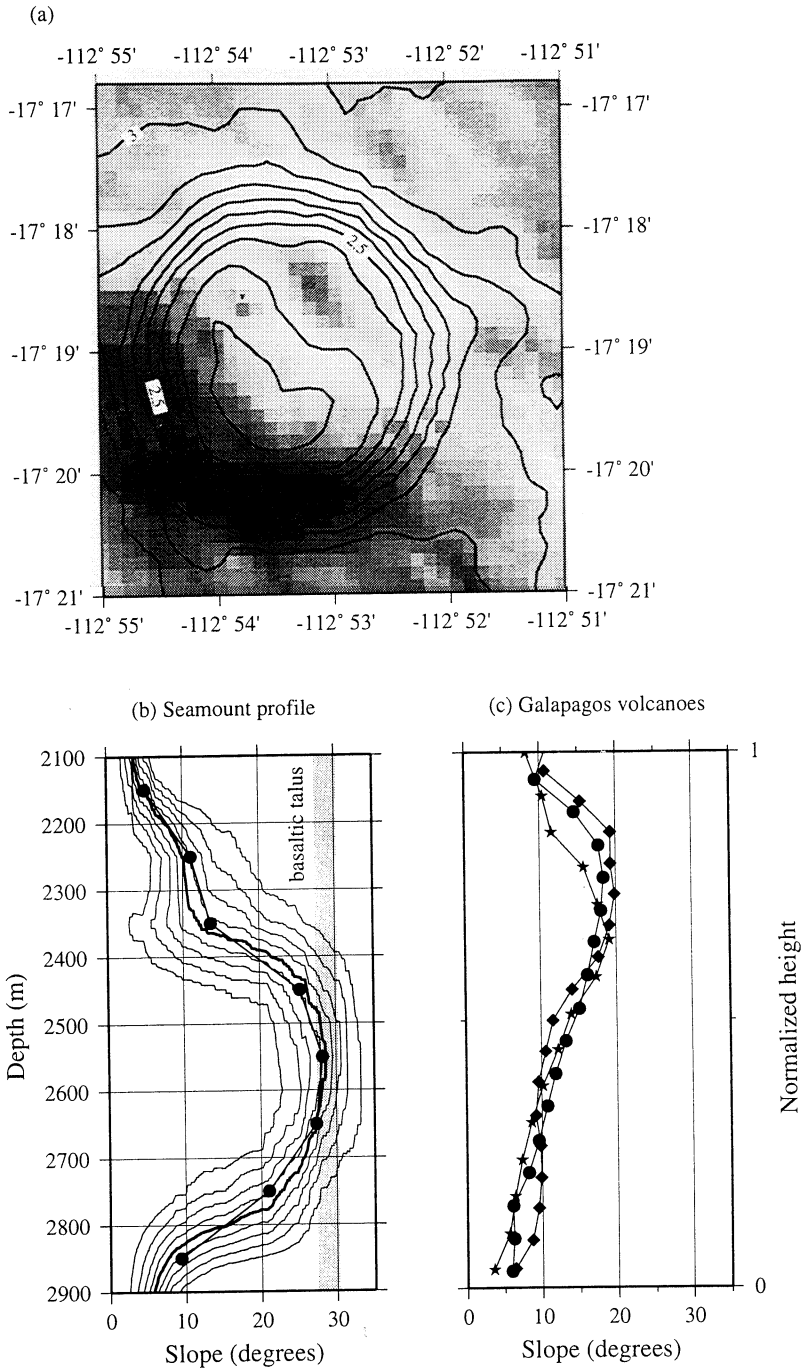

Figure 11. (a) A typical flat-topped volcano of the southern East Pacific Rise [*Scheirer et al.*, 1996]. (b) Slope profile representation of the volcano showing successive 10% levels of the slope distribution (fine lines), median slope (bold line), and mean slope (solid circles). The shaded line near 30° represents the slopes of basaltic talus ramps measured from submersible dive profiles [*Mitchell et al.*, 2000] showing that the flanks are probably talus ramps as often observed [*Fornari et al.*, 1984; *Batiza et al.*, 1989]. Above 2400 m, the summit is not perfectly flat but is irregular. (c) Mean slope profiles of Galapagos volcanoes [*Mouginis-Mark et al.*, 1996]. Symbols represent the three "inverted soup-bowl"-shaped volcanoes: Wolf (diamonds), Cerro Azul (circles), and Fernandina (stars). The profiles, in contrast to oceanic volcanoes, show steepening toward summits and a relatively abrupt summit transition. The lower slopes of Galapagos volcano aprons reflect the greater mobility of subaerial lava [*Simkin*, 1972].

measurements [*Batiza and Vanko*, 1983; *Clague et al.*, 2000a; *Hammond*, 1997]. If calderas are caused by collapse into magma chambers involving near-vertical ring faults [*Batiza et al.*, 1984; *Gudmundsson*, 1998a; *Lipman*, 1997; *Roche et al.*, 2000], their diameters reflect the diameters of their underlying magma bodies. Figure 14a shows negligible correlation of caldera diameters with edifice height, suggesting that these high-level magma chambers are only late stage residual bodies that do not supply the whole edifice volume, at least not in a single event [*Batiza and Vanko*, 1983; *Hammond*, 1997], as also implied by geochemical diversity

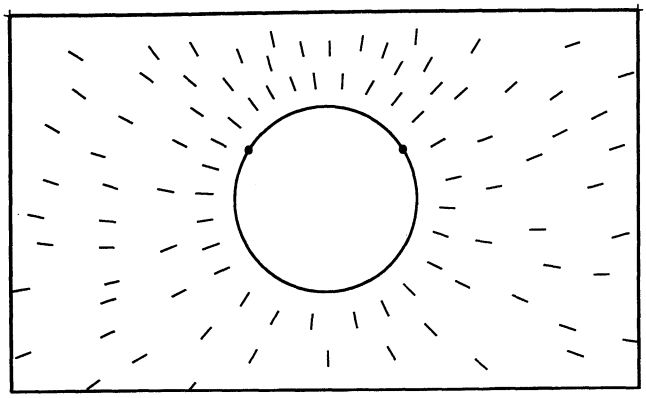

Figure 12. Upper part of *Gudmundsson's* [1998b, Figure 12] model representing stresses around magma chambers beneath Icelandic central volcanoes. Lines represent the orientations of maximum compressive stress in elastic material with excess fluid pressure in the central cavity as the only loading. The points of smallest compressive stress tangential to the cavity walls, marked by the two solid circles, are where sheets are most likely to escape from the magma chamber. The maximum compressive stress orientation there, dipping ~45°, corresponds to the mean dip of inclined sheets mapped in eroded Icelandic central volcanoes [*Gautneb and Gudmundsson*, 1992].

of lavas from individual seamounts [*Allan et al.*, 1987; *Zindler et al.*, 1984]. The following statistic calculated from the data in Figure 14a has R=0.19:

$$R = \frac{\sum_i (x_i - \bar{x})(y_i - \bar{y})}{\sqrt{\sum_i (x_i - \bar{x})^2 \sum_i (y_i - \bar{y})^2}}, \quad (3)$$

where x_i and y_i are the ordinate and coordinate values of the data and $\bar{x}$ and $\bar{y}$ are their mean values. Figure 14b, however, shows a weak correlation with summit diameters (R=0.43), implying that summit diameters partly reflect the size of their underlying magma bodies. Only a weak correlation is expected if the flat tops of volcanoes are generated by eruptive cone sheets when their chambers are overpressured, since their chamber dimensions are not necessarily the same as those during the later collapse stage creating the calderas.

The possibility that different modes of eruption lead to different shapes has a number of consequences. For example, the increasing density of oceanic layer 2A with age implied by seismic velocities [*Grevemeyer and Weigel*, 1997; *Carlson*, 1998] and gravity measurements [*Holmes and Johnson*, 1993] suggests that this horizon will become less able to act as a density trap, and it probably also becomes less of a freezing barrier owing to lower permeability and less vigorous hydrothermal cooling. The result should be fewer laccolith intrusions and fewer flat-topped new volcanoes on old seafloor. This is difficult to test from seamount shape statistics because mean volcano height also increases with seafloor age [*Abers et al.*, 1988] and tall volcanoes (>1000 m) have sharp peaks [*Smith*, 1988]. It is interesting to note, however, that short (<1000 m tall) new volcanoes in the Society and Austral hotspot regions on much older seafloor have sharp peaks [*Binard et al.*, 1992].

The height distribution of oceanic seamounts is commonly an exponential [*Abers et al.*, 1988; *Jordan et al.*, 1983; *Rappaport et al.*, 1997; *Scheirer and Macdonald*, 1995; *Smith*, 1996; *Smith and Jordan*, 1988], reflecting the increasingly fewer numbers of seamounts with increasing height. The exponential height distribution has been interpreted using a magmastatic head model to infer the distribution of source depths [*Smith and Cann*, 1992], but as explained below, flat summits of seamounts may not represent the limit of magma pressure. The height of a volcano reflects both the volume of magma erupted and the geometry of eruption, so the fact that the distribution is exponential may have no particular meaning since it reflects a complicated result of eruption volumes and geometries. Alternatively, the volume distribution should be interesting in its own right because assuming that small volcanoes are monogenetic [*Batiza and Vanko*, 1983], their volume distribution should reflect the sizes of melt packets that have both penetrated the lithosphere and erupted. Figure 15 shows the cumulative volume distribution for northern East Pacific Rise (EPR) seamounts [*Scheirer and Macdonald*, 1995], which shows that the data can be approximated by a power law of the form $N(v>V) \propto V^{-0.68}$. (More accurate volume estimates will be needed to assess the shape of the volume distribution so the power law model is not necessarily preferred but is included for illustration.)

5.1.2. Caldera infill model and caldera wall morphology. *Clague et al.* [2000a] suggested that large circular calderas are

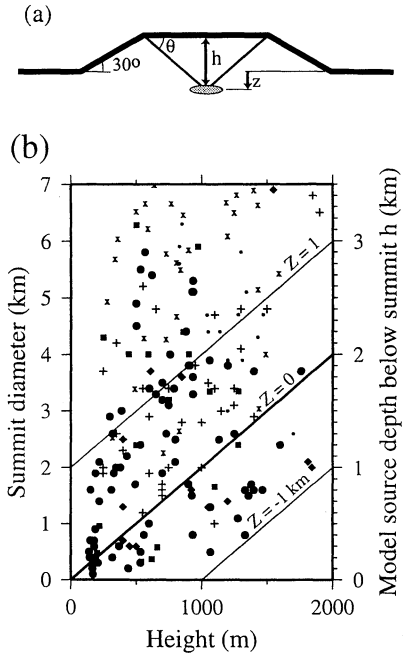

Figure 13. (a) Model for flat-topped mid-ocean ridge volcanoes in which the flat summit is created by flows emitted from cone sheets sourced from a shallow magma body. The diagonal lines represent only the outermost eruptive cone sheets (other sheets omitted for clarity). (b) Summit diameters taken from *Batiza and Vanko* [1983] (squares), *Smith* [1988] (large circles), *Clague et al.* [2000a] (small circles), *Binard et al.* [1992] (diamonds), *Scheirer and Macdonald* [1995] (pluses) and *Hammond* [1997] (crosses). The scale on the right shows inferred magma source depth, h, assuming the geometry in Figure 13a and an outermost eruptive cone sheet dip of 45°. Oblique lines show the magma body depth Z relative to underlying oceanic basement top, suggesting that most bodies lay within the upper basement (data deeper than Z=0), and probably within the upper oceanic crust. According to the model the dispersion of the data implies that intrusion depth Z and/or cone sheet or magma body geometry are not uniform.

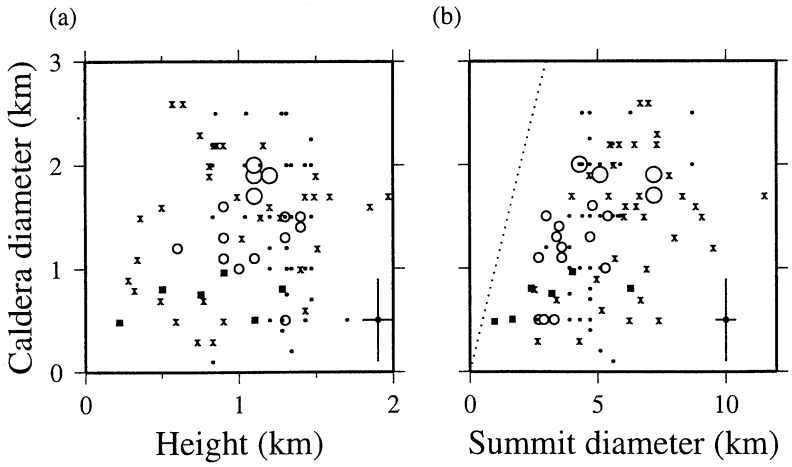

Figure 14. Caldera and crater diameters of mid-ocean ridge volcanoes from *Batiza and Vanko* [1983] (solid squares), *Hammond* [1997] (crosses), *Clague et al.* [2000a] (small solid circles), and measurements made here from East Pacific Rise multibeam sonar data sets (open circles) [*Cochran et al.*, 1993; *Scheirer et al.*, 1996]. Large open circles represent measurements where side-scan sonar images were available [*Barone and Ryan*, 1990] to more accurately constrain diameters. (a) Variation with edifice height showing negligible correlation. (b) Variation with summit diameter showing a weak correlation, possibly implying a connection between size of late stage high-level magma chambers and summit diameters. Error bars at lower right represent the maximum uncertainties of the new measurements made here where not constrained by side-scan sonar images. The summit diameters of *Hammond* [1997] were computed from his table of basal diameters, heights, and flank slopes. The dotted line corresponds to equal summit and caldera diameters; since the data occur away from this line, the correlation is not an artifact of calderas being necessarily smaller than their associated summits.

created at an early stage of seamount growth and subsequently filled in and overflowed by lava. With repeated collapse and caldera infill, edifices grow with flat-tops and circular outlines, a suggestion similar to one made earlier by *Searle* [1983]. *Clague et al.*'s new high-resolution bathymetry reveals that summits commonly have low-relief lava shields (implying eruption from central vents) that are cut by later calderas. The results show that infill of early calderas can contribute to the truncated cone form.

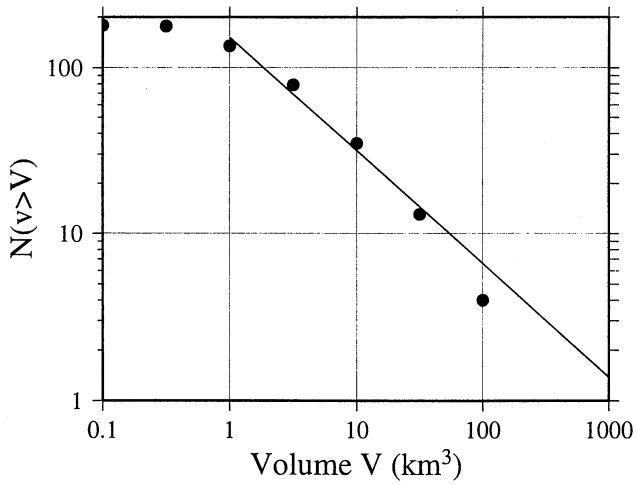

Figure 15. Cumulative distribution of the mid-ocean ridge seamount volumes measured by *Scheirer and Macdonald* [1995]. The straight line is a regression for volumes of 1-32 km^3, suggesting that intermediate size seamounts might be represented by a power law distribution with exponent 0.68. Deviations from the power law model for smaller or larger volumes suggest that the model is inappropriate or reflect problems of population sampling.

It is unclear, however, if all flat-topped seamounts are created solely by caldera infill, and the presence of cone sheet complexes in comparable volcanoes in ophiolites, Iceland, and the Galapagos suggests that intrusions should also have a role. Furthermore, later calderas have diameters much smaller than their associated summit plateaux (data in Figure 14b fall far to the right of the dotted line with no caldera diameters similar to summit diameters). Nevertheless, *Clague et al.* [2000a] also interpret the simple ring fault boundaries of summit calderas as implying shallow magma chamber depths by comparison of their morphologies with results of analogue experiments [*Rocke et al.*, 2000], and they observe that calderas commonly cut the volcano walls. These observations imply that magma chambers lie within the shallow underlying basement, an interpretation that is consistent with magma chambers lying within upper oceanic crust, as described above.

5.1.3. Other proposed origins *McBirney and Williams* [1969] suggested that the steep upper slopes of Galapagos volcanoes could partly reflect doming over intruding sills or laccoliths. *Cullen et al.* [1987] used a simple elastic mechanical model to show that doming was a viable mechanism provided that intrusions are shallow. Although the flat tops of seamounts are not explained by this mechanism and caldera formations of at least one of the Galapagos volcanoes supports a constructional rather than inflation origin [*Naumann and Geist*, 2000], doming is suspected to contribute to seamount growth because some interpreted seamounts in ophiolites contain numerous sills [e.g., *MacPherson*, 1983]. The *Cullen et al.* [1987] model predicts that the breadth of doming reflects the intrusion width; if the widths of the summit plateaux reflect their breadths of doming, the correlation in Figure 14b might be expected from this model. This mechanism would also support the contention made here that mid-ocean ridge seamounts are supplied from magma bodies within the shallow oceanic crust.

Barone and Ryan [1990] suggested that volcanoes grow to heights that reflect the pressure available in magma chambers to drive eruption and then grow outward to create flat summits. It is unclear, however, how surface lateral growth could occur if the magma is at its pressure limit, and it is unclear why lateral growth would lead to circular shapes. *Wilson et al.* [1992] also point out difficulties with the magma head model which cast doubt on magma pressure control. *Searle* [1983] attributed the flat top form to the high mobility of lavas erupted from central vents, while the steep margins represent brecciated flow fronts, but it is also unclear how this would lead to the near-circular plan view geometry and many flat-topped volcanoes are more than 1000 m high, much taller than typical submarine flows [*Moore and Chadwick*, 1995].

5.2. Origins of Transition to Stellate Edifices

Although several factors cause the transition, the lack of additional data precludes a multiparameter analysis which might help to isolate them (reliable radiometric dates, for example, would be useful to address effects of long-term erosion). The variation with edifice height (Figure 6) implies that height is an important parameter, however.

5.2.1. Role of central magma bodies. The 3-km transition height coincides with depths of magma chamber tops on Hawaii, Reunion, and beneath Krafla volcano [*Ryan*, 1987; *Nercessian et al.*, 1996]. Morphologic complexity for edifices taller than 3 km could therefore arise because of effects where magma bodies lie above edifice base (Figure 16) [*Head and Wilson*, 1992]. If magma bodies lie close to the horizon of neutral buoyancy (HNB), lateral dikes intruded from them are expected to escape along the HNB [*Lister and Kerr*, 1991]. Where dikes overshoot the HNB to the edifice surface, a pressure difference between the magma reservoir and surrounding seawater is available to drive flank eruptions (Figure 16). Eruption from deeper magma bodies involves transport by vertical feeder dikes before lateral intrusion [*Lister and Kerr*, 1991], which is less efficient owing to the work against gravity and longer viscous path. Vertical transport from deep magma bodies is also more likely to lead to volatile exsolution, density reduction, and further ascent and eruption, rather than to lateral intrusion. The importance of pressure gradients was shown by *Rubin and Pollard* [1987], who noted that the slope of the east rift zone of Kilauea suggests a pressure gradient in dikes intruding parallel to the surface that is consistent with the idea that viscous pressure loss controls the long-term slope of rift zones. The steeper submarine slopes of volcanoes compared to their subaerial slopes could partly reflect the lower pressure difference available to drive flank eruptions [*Lonsdale*, 1989; *Fialko and Rubin*, 1999]. *Lacey et al.* [1981] similarly proposed that flank slopes reflect a balance between viscous pressure loss in fractures compared to the gravitational work done raising magma to the surface. High-level intrusions may trigger landslides because they can oversteepen flank slopes, their associated seismicity causes ground shaking [*Moore et al.*, 1989], and heating of groundwater and magmatic fluids can create pore fluid overpressure triggering collapse [*Elsworth and Voight*, 1995].

Gas exsolution further modifies the above argument. *Carrigan et al.* [1992] pointed out that exsolved gas in a vertically intruding dike reduces the dike's average density and hence reduces its magmastatic pressure, allowing lithostatic pressure on the underlying chamber to drive eruption. CO_2 exsolves at high pressure and can occur in significant amounts in hotspot magmas. For example, *Dixon et al.* [1997] estimated that giant flows north of Hawaii had 2.0-5.4 wt % CO_2, which may have been sufficient to produce lava fountaining even at their 4600 m eruption depth [*Clague et al.*, 2000b]. The reduced density associated with gas exsolution is more likely to encourage ascent of magma rather than lateral intrusion in rift zones (Figure 16) or to encourage ascent and premature eruption where dikes do intrude rift zones. Below sea level, dikes intruding downrift parallel to the edifice surface will experience increasing ambient pressure, causing resorption of gases and reducing susceptibility to erupt by gas drive. Volatile contents in magmas of Kilauea's submarine Puna Ridge are significantly low [*Dixon et al.*, 1991] probably because magma beneath the summit of Kilauea goes through cycles of eruption and return of degassed lava from lava lakes to the shallow summit chamber before intruding down the ridge [*Clague et al.*, 2000b]. The dramatically increasing lengths of rift zones in Figure 9 for edifices above 5000 m height, which *Vogt and Smoot* [1984] attributed to low-viscosity magmas, could therefore instead be due to volcanoes rising above sea level and degassing magma by shallow recycling. Such high-density degassed magmas are then less prone to gas-driven eruption and promote rift zone growth in the largest edifices, contributing to the more extreme stellate forms.

5.2.2. Age-dependent effects. The edifices in Figure 3 that are smaller than 1400 m are almost all younger than 5 Ma (the age of their underlying oceanic crust), whereas the large edifices have a wider range of ages, so the transition in Figure 6 could potentially be an artifact of different edifice ages rather than heights. By analogy with erosion of mid-ocean ridge fault scarps [*Tucholke et al.*, 1997], erosion might be expected to cause small seamounts to develop gullies and a fine crenulation of contours. The large seamounts here, however, are represented by smoothed contours so erosion probably does not greatly affect the transition value. *Keating* [1998] described giant landslides on old edifices, and *Lopez and Williams* [1993] attribute landsliding in some continental volcanoes to weakening by hydrothermal alteration of volcanic rocks to clays, a process that could continue long after volcanic activity. Such landslides could potentially affect the resolved transition height if they are common. Sonar imagery

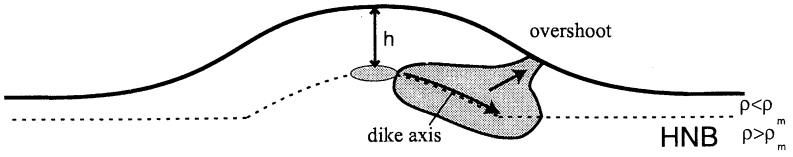

Figure 16. If magma bodies lie close to the horizon of neutral buoyancy (HNB), lateral dikes are expected to escape along the HNB [*Lister and Kerr*, 1991]. Where dikes overshoot the HNB to the edifice surface, a pressure difference between the magma source and seawater is available to drive flank eruptions. Efficiency of volcanic rift zone growth, and hence morphologic complexity, may therefore be related to the upper level of magma bodies, which lie above base for the largest edifices.

from Hawaii, however, shows most recent landslides occur around the youngest islands [*Moore et al.*, 1994] so landsliding is expected to be most common generally during the early growth stage. *Bridges* [1997] describes sonar images of small Cretaceous seamounts near Hawaii showing generally round edifices with only five out of 380 seamounts with diameters smaller than 20 km (heights below 2 km) interpreted as star-shaped.

5.2.3. Other factors related to edifice height. Most small seamounts are probably monogenetic, whereas large seamounts grow over long periods with more complex eruption and deformation histories [*Batiza and Vanko*, 1983; *Fornari et al.*, 1987], so the irregularity of some large seamounts is due to the fact that they can consist of more than one volcano. Rift zones in large edifices do not generally coincide with basement structures [*Fiske and Jackson*, 1972], whereas features in small seamounts aligned with basement faults imply some effect on eruption geometry [*Batiza and Vanko*, 1983; *Fornari et al.*, 1987]. Although both mid-ocean ridge and intraplate seamounts are constructed largely from tholeiitic and alkaline basaltic magmas [*Batiza and Vanko*, 1984], some systematic compositional differences might be expected which could potentially affect magma physical properties. Where seamounts are tall enough to erupt in shallow water, explosive interaction of magma with seawater produces friable hyaloclastite which is susceptible to shallow landsliding [*Staudigel and Schmincke*, 1984], an effect that could enhance variability above ~4 km height but probably does not affect the 3-km transition value. The Halina Slump in Hawaii involves flank movement over a decollement in pelagic sediments beneath the Kilauea edifice [*Moore et al.*, 1989], and flank movement has been proposed to facilitate growth of volcanic rift zones [*Dieterich*, 1988]. If flank movement is more generally important, it could preferentially affect edifices growing over thick hemipelagic clay, enhancing morphologic variability of the tallest edifices because they are more common on older, thickly sedimented seafloor [*Vogt*, 1974]. *Wyss* [1980] proposed that rift zones grow in large edifices in response to tangential stretching over buoyant mantle plumes. While this may be important for the largest edifices, typical lithospheric elastic thicknesses of 10-40 km [*Watts et al.*, 1980] imply that deformation is spread over 200-500 km, so localized stretching beneath moderate-sized 3-km-high edifices is not significant.

Stresses caused by spreading of volcanoes under gravity increase with edifice size until they exceed the cohesive strength of the rock and promote fracturing, encouraging landsliding. *Sturgul and Grinshpan* [1976] modeled stresses in a 1-km-high mountain with 60° slopes assuming elastic deformation and using measured physical properties. Their model predicted tensional stresses at the mountain summit and margins. Similar stresses around the margins of small seamounts (30° in Figure 11) could potentially encourage rock fragmentation and the formation of talus slopes. However, volcanic materials have poor cohesion owing to pervasive fracturing [*Iverson*, 1995]. *Borgia* [1994] modeled stresses with more realistic flank slopes and found that elastic models predicted compression everywhere. Her models predicted widespread extension only when they incorporated an underlying decollement and viscous core to represent the effect of hot intrusions, which are only expected to be important for the large edifices such as Hawaii [*Clague and Denlinger*, 1994].

5.3. Controls on Magma Chamber Depths

The above interpretations involve magma chambers within upper oceanic crust for small volcanoes but above oceanic basement for the larger volcanoes, with the position of the chamber rising approximately with the horizon of neutral buoyancy (HNB). The idea of buoyancy control is reconsidered here, and given shortcomings of the simple buoyancy model, it is suggested that cooling by hydrothermal convection could instead control magma chamber levels in a way that mimics buoyancy control. *Clague and Dixon* [2000] have similarly suggested that thermomechanical properties of the crust control positions of Hawaiian shallow magma chambers.

Ryan [1987] and *Walker* [1989] defined the HNB as the surface where magma density equals the surrounding bulk rock density. Crack closure with increasing lithostatic pressure causes density to increase with depth so rock above and below the HNB has lower and higher density, respectively, compared to the magma. Magma buoyancy relative to the host rock was envisaged to trap magma at the HNB. As a volcano grows, crack closure with increasing lithostatic pressure, intrusion of dense dikes, and crystallization of dense minerals in magma chambers cause the HNB to rise, tracking the growing summit and causing magma bodies to pond at higher levels.

The HNB depth within seamounts can be roughly assessed from seismic velocity measurements. The bold line in Figure 17a

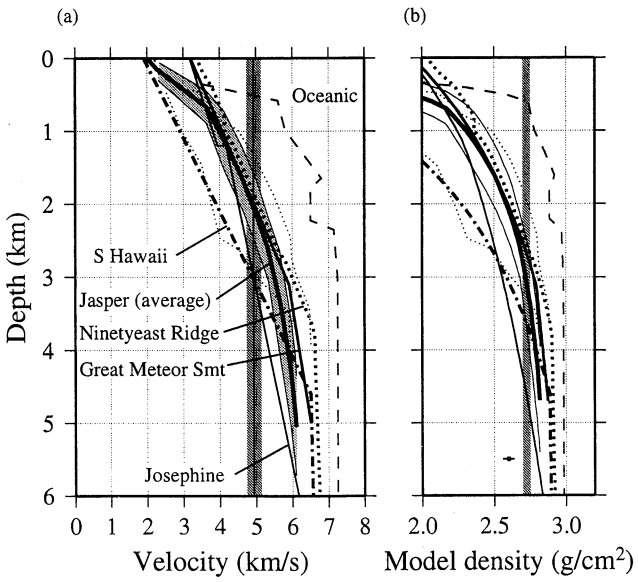

Figure 17. (a) Seismic *P* wave velocity models of submarine volcanic edifices (south Hawaii [*Klein*, 1981], Jasper Seamount [*Hammer et al.*, 1994], Ninetyeast Ridge [*Grevemeyer et al.*, 1998], Great Meteor Seamount [*Weigel and Grevemeyer*, 1999], and Josephine Seamount [*Peirce and Barton*, 1991]). The dashed line represents typical 0.2 Ma fast-spread oceanic crust [*Vera et al.*, 1990]. The Jasper Seamount profile (heavy bold line with lightly shaded 2σ uncertainty bounds) is the reference (average) velocity model profile and the light dotted lines illustrate variability between opposite flanks [*Hammer et al.*, 1994]. Vertical dark shaded line (4.93 km/s) represents an average velocity of 5.9 Ma oceanic extrusives at Ocean Drilling Program Site 504B [*Swift et al.*, 1996], which corresponds to 10% average porosity [*Becker et al.*, 1988] and is used as a reference velocity in the text. (b) Bulk rock density calculated using a density-slowness regression [*Carlson and Herrick*, 1990] from the velocity models in Figure 17a. Horizontal bar represents typical uncertainty in the regression [*Carlson and Herrick*, 1990] not velocity model uncertainty. Shaded line (2.70-2.75 g/cm^3) is the expected density of basaltic melt [*Stolper and Walker*, 1980]. From these data the horizon of neutral buoyancy occurs at 3.3 km average depth.

shows the mean P wave velocity structure of Jasper Seamount [*Hammer et al.*, 1994], a typical volcanic edifice formed mostly during 11.5-10.5 Ma on seafloor originally 13 Ma old [*Gee et al.*, 1991]. The seamount is 3500 m high, so it lies within the morphologic transition. The seamount velocities are everywhere less than typical oceanic crust (dashed line in Figure 17a) and suggest that the volcano largely consists of extrusive rocks [*Hammer et al.*, 1994]. The other lines show similar velocities through other submarine edifices. Velocities <5 km/s are also typical of the flanks of volcanic ocean islands to depths of 2 km or more [*Caress et al.*, 1995; *Charvis et al.*, 1999; *Hill and Zucca*, 1987; *Watts et al.*, 1997; *Weigel and Grevemeyer*, 1999]. For reference, the vertical dark shaded line (4.93 km/s) is the mean velocity in 5.9 Ma extrusive rocks at Ocean Drilling Program Site 504B [*Swift et al.*, 1996] at 360 to 480 m depth, which corresponds to 10±1% mean porosity [*Becker et al.*, 1988]. Assuming a basaltic melt density of 2.70 to 2.75 g/cm^3 [*Stolper and Walker*, 1980], this velocity lies at the low end of the 10-13% porosity range predicted for the HNB (assuming 2.95 and 1.03 g/cm^3 grain and pore water density). Because lithostatic pressure preferentially closes elongated cracks, increasing velocity disproportionately to porosity [*Walsh*, 1965], the velocity corresponding to 10% porosity in seamount edifices is more than 5 km/s [*Wilkens et al.*, 1991] and the HNB is expected to lie deeper than 2 to 3 km within edifices such as Jasper. Figure 17b shows densities calculated from the velocity models using a density-slowness regression derived from laboratory samples [*Carlson and Herrick*, 1990], which was shown to be representative of in situ conditions. Model densities exceed 2.70 to 2.75 g/cm^3 (shaded line) at 3.1 km for Jasper and at 3.3 km on average for all profiles. The density contrast between magma and bulk rock suggests that buoyancy effects are greatest at depths <2 km, suppressing magma rise, but less efficient deeper than 2 km.

A difficulty with the HNB concept applied to magma chambers is that it assumes that a buoyancy effect between magma and surrounding solid can drive bulk movement of the magma. It has been argued that individual dikes can intrude along the HNB [*Lister and Kerr*, 1991], which might be envisaged to inflate, creating a chamber at that depth. However, intrusion of one dike will affect the stress state for subsequently intruding dikes, and other sources of loading will affect dike intrusion depth [*Rubin and Pollard*, 1987]. Figure 17b also suggests only weak buoyancy at depths >2 km. In contrast, mid-ocean ridge magma chambers lie deeper than the HNB [*Hooft and Detrick*, 1993], and their depths inversely correlate with spreading rate [*Purdy et al.*, 1992], so rising magma is arrested below the HNB at a depth that is thermally controlled. *Phipps Morgan and Chen* [1993] proposed that latent energy from continuously accumulating melt beneath ridges is balanced by hydrothermal cooling, leading to a steady state freezing horizon. *Smith and Cann* [1992] similarly proposed that chambers beneath small mid-ocean ridge seamounts occur at the thermally controlled brittle-ductile transition. Deeper magma chambers will be less efficiently cooled by hydrothermal circulation and so reflect smaller rates of latent heat and melt supplied to the chamber. According to this mechanism, slowly rising magma beneath seamounts freezes where it encounters hydrothermal fluids, generating an impermeable horizon that traps further magma below it, creating a magma chamber. Chamber depths then appear to lie near the HNB if permeability of the high-porosity upper crust leads to penetration depths of hydrothermal circulation and a freezing horizon near the HNB. Chamber depths are likely to vary, dependent on their rate of magma supply and chamber ceiling permeability structures.

6. Conclusions

Submarine volcanoes grow from simple conical forms (volcanoes <1 km tall) to stellate forms with increasing edifice height, where the stellate form reflects the relief of radiating volcanic rift zones and embayments created by massive landslides. The analysis based on the midheight contour suggests that the transition is gradual and occurs when the volcanoes reach 2-4 km height (best estimate 3.0 km). Tall volcanoes have a variety forms (some are stellate and others more rounded), suggesting complex processes affecting their growth. The 3-km transition height coincides with the depth of the top of magma chambers within ocean basin volcanic islands, so it is inferred that the morphological change arises where volcanoes growing above 3 km height have magma chambers lying above their basement. Such high level magma chambers more efficiently feed flank rift zones, and intrusions from them promote flank collapse via groundwater heating or slope oversteepening.

Small mid-ocean ridge volcanoes have truncated cone shapes. The most likely eruption mechanisms leading to these shapes involve early caldera formation and infill [*Clague et al.*, 2000a] or (as explored here) eruption from cone sheets. The magma chamber sources of such eruptions lie within the upper oceanic crust (shallower than 2 km) rather than significantly deeper. This shallow chamber depth for small volcanoes and the 3-km depth of the transition to the stellate form implying 3 km deep chambers beneath tall volcanoes are consistent with buoyancy control on the level of magma chambers (since the 3-km transition coincides with the depth to the horizon of neutral buoyancy inferred from seismic velocity measurements). This is probably a coincidence, however. Hydrothermal circulation through the permeable upper oceanic crust has been proposed to modulate depths of mid-ocean ridge magma chambers [*Phipps Morgan and Chen*, 1993] and could also lead to shallow chamber depths beneath seamounts. Different permeability structures of chamber ceilings and different rates of magma supply will lead to more varied chamber depths than predicted from the buoyancy model. Varied chamber depths are consistent with some morphological observations of mid-ocean ridge seamounts, and their associated varied ambient pressures imply that different evolutionary trends in erupted lavas can be expected.

Acknowledgments. This study is based on data made freely available in public databanks, in particular the multibeam synthesis at Lamont-Doherty Earth Observatory (http://www.imager.ldeo.columbia.edu/ridge). The west coast U.S. multibeam data were mostly collected by ships of the National Oceanographic and Atmospheric Administration. I thank D. G. Masson and A. B. Watts for access to the sonar data from El Hierro collected during RRS *Charles Darwin* cruise 108 (funded by the Natural Environment Research Council, U.K.). The subaerial terrain model of El Hierro was created by M. J. R. Gee. Many of the figures here were produced with the GMT software system [*Wessel and Smith*, 1991]. I am also grateful to I. Grevemeyer for prepublication seismic velocities used in Figure 17 and W. Sager for copies of seamount maps. This work benefited from discussions with R. S. J. Sparks, A. B. Watts, M. J. R. Gee and D. G. Masson, and constructive reviews by A. McBirney, P. Vogt, C. Oppenheimer, L. Kirstein, and an anonymous reviewer. Support provided by a Royal Society University Research Fellowship is very gratefully acknowledged.

References

Abers, G.A., B. Parsons, and J.K. Weissel, Seamount abundances and distributions in the southeast Pacific, *Earth Planet. Sci. Lett.*, *87*, 137-151, 1988.

Allan, J.F., R. Batiza, and P. Lonsdale, Petrology and geochemistry of lavas from seamounts flanking the East Pacific Rise axis, 21°N: Implications concerning the mantle source composition for both

seamount and adjacent EPR lavas, in *Seamounts, Islands and Atolls, Geophys. Monogr. Ser.*, vol. 43, edited by B.H. Keating et al., pp. 255-282, AGU, Washington, D. C., 1987.

Barone, A.M., and W.B.F. Ryan, Single plume model for asynchronous formation of the Lamont Seamounts and adjacent East Pacific Rise terrains, *J. Geophys. Res.*, *95*, 10,801-10,827, 1990.

Batiza, R., and D. Vanko, Volcanic development of small oceanic central volcanoes on the flanks of the East Pacific Rise inferred from narrow-beam echo-sounder surveys, *Mar. Geol.*, *54*, 53-90, 1983.

Batiza, R., and D. Vanko, Petrology of young Pacific seamounts, *J. Geophys. Res.*, *89*, 11,235-11,260, 1984.

Batiza, R., D.J. Fornari, D.A. Vanko, and P. Lonsdale, Craters, calderas, and hyaloclastites on young Pacific seamounts, *J. Geophys. Res.*, *89*, 8371-8390, 1984.

Batiza, R., T.L. Smith, and Y. Niu, Geological and petrological evolution of seamounts near the EPR based on submersible and camera study, *Mar. Geophys. Res.*, *11*, 169-236, 1989.

Becker, K., et al., *Proceedings of the Ocean Drilling Program, Initial Reports, Part A,* vol. 111, Ocean Drill. Program, College Station, Tex., 1988.

Binard, N., R. Hekinian, J.L. Cheminee, and P. Stoffers, Styles of eruptive activity on intraplate volcanoes in the Society and Austral hot spot regions: Bathymetry, petrology, and submersible observations, *J. Geophys. Res.*, *97*, 13,999-14,015, 1992.

Borgia, A., Dynamic basis of volcanic spreading, *J. Geophys. Res.*, *99*, 17,791-17,804, 1994.

Bridges, N.T., Characteristics of seamounts near Hawaii as viewed by GLORIA, *Mar. Geol.*, *138*, 273-301, 1997.

Bryan, W.B., S.E. Humphris, G. Thompson, and J.F. Casey, Comparative volcanology of small axial eruptive centers in the MARK area, *J. Geophys. Res.*, *99*, 2973-2984, 1994.

Caress, D.W., M.K. McNutt, R.S. Detrick, and J.C. Mutter, Seismic imaging of hotspot-related crustal underplating beneath the Marquesas Islands, *Nature*, *373*, 600-603, 1995.

Carlson, R.L., Seismic velocities in the uppermost oceanic crust: Age dependence and the fate of layer 2A, *J. Geophys. Res.*, *103*, 7069-7077, 1998.

Carlson, R.L., and C.N. Herrick, Densities and porosities in the oceanic crust and their variations with depth and age, *J. Geophys. Res.*, *95*, 9153-9170, 1990.

Carracedo, J.C., The Canary Islands: An example of structural control on the growth of large oceanic-island volcanoes, *J. Volcanol. Geotherm. Res.*, *60*, 225-241, 1994.

Carrigan, C.R., G. Schubert, and J.C. Eichelberger, Thermal and dynamical regimes of single- and two-phase magmatic flow in dikes, *J. Geophys. Res.*, *97*, 17,377-17,392, 1992.

Chadwick, W.W., and J.H. Dieterich, Mechanical modeling of circumferential and radial dike intrusion on Galapagos volcanoes, *J. Volcanol. Geotherm. Res.*, *66*, 37-52, 1995.

Charvis, P., A. Laesanpura, J. Gallart, A. Hirn, J.-C. Lepine, B. de Voogd, T.A. Minshull, Y. Hello, and B. Pontoise, Spatial distribution of hostpot material added to the lithosphere under La Reunion, from wide-angle seismic data, *J. Geophys. Res.*, *104*, 2875-2893, 1999.

Clague, D.A., and R.P. Denlinger, Role of olivine cumulates in destabilizing the flanks of Hawaiian volcanoes, *Bull. Volcanol.*, *56*, 425-434, 1994.

Clague, D.A., and J.E. Dixon, Extrinsic controls on the evolution of Hawaiian ocean island volcanoes, *Geochem. Geophys. Geosyst.*, *1*, Paper number 1999GC000023, 2000.

Clague, D.A., J.R. Reynolds, and A.S. Davis, Near-ridge seamount chains in the northeastern Pacific Ocean, *J. Geophys. Res.*, *105*, 16,501-16,561, 2000a.

Clague, D.A., J.G. Moore, and J.R. Reynolds, Formation of flat-topped volcanic cones in Hawai'i, *Bull. Volcanol.*, *62*, 214-233, 2000b.

Cochran, J.R., J.A. Goff, A. Malinverno, D.J. Fornari, C. Keeley, and X. Wang, Morphology of a 'superfast' mid-ocean ridge crest and flanks: The East Pacific Rise, 7°-9°S, *Mar. Geophys. Res.*, *15*, 65-75, 1993.

Cullen, A.B., A.R. McBirney, and R.D. Rogers, Structural controls on the morphology of Galapagos shields, *J. Volcanol. Geotherm. Res.*, *34*, 143-151, 1987.

Dixon, J.E., D.A. Clague, and E.M. Stolper, Degassing history of water, sulfur, and carbon in submarine lavas from Kilauea, Hawaii, *J. Geol.*, *99*, 371-394, 1991.

Dixon, J.E., D.A. Clague, P. Wallace, and R. Poreda, Volatiles in alkalic basalts from the North Arch Volcanic Field, Hawaii: Extensive degassing of deep submarine-erupted alkalic series lavas, *J. Petrol.*, *38*, 911-939, 1997.

Dieterich, J.H., Growth and persistence of Hawaiian volcanic rift zones, *J. Geophys. Res.*, *93*, 4258-4270, 1988.

Eddy, C.A., Y. Dilek, S. Hurst, and E.M. Moores, Seamount formation and associated caldera complex and hydrothermal mineralization in ancient oceanic crust, Troodos ophiolite (Cyprus), Tectonophys., *292*, 189-210, 1998.

Elsworth, D., and B. Voight, Dike intrusion as a trigger for large earthquakes and the failure of volcano flanks, *J. Geophys. Res.*, *100*, 6005-6024, 1995.

Ewing, J.I., M. Ewing, T. Aitkin, and W.J. Ludwig, North Pacific sediment layers measured by seismic profiling, in *The Crust and Upper Mantle of the Pacific Area*, *Geophys. Monogr. Ser.*, vol. 12, edited by L. Knopoff, C.L. Drake, and P.J. Hart, pp. 147-173, AGU, Washington, D. C., 1968.

Fialko, Y.A., and A.M. Rubin, What controls the along-strike slopes of volcanic rift zones?, *J. Geophys. Res.*, *104*, 20,007-20,020, 1999.

Fiske, R.S., and E.D. Jackson, Orientation and growth of Hawaiian volcanic rifts: The effect of regional structure and gravitational stresses, *Proc. R. Soc. London, Ser. A*, *329*, 299-326, 1972.

Fornari, D.J., W.B.F. Ryan, and P.J. Fox, The evolution of craters and calderas on young seamounts: Insights from Sea MARC I and Sea Beam sonar surveys of a small seamount group near the axis of the East Pacific Rise at ~10°N, *J. Geophys. Res.*, *89*, 11,069-11,083, 1984.

Fornari, D.J., R. Batiza, and J.F. Allan, Irregularly shaped seamounts near the East Pacific Rise: Implications for seamount origin and rise axis processes, in *Seamounts, Islands and Atolls, Geophys, Monogr. Ser.,* vol. 43, edited by B.H. Keating, P. Fryer, R. Batiza, and G.W. Boehlert, pp. 35-47, AGU, Washington, D. C., 1987.

Fornari, D.J., M.R. Perfit, J.F. Allan, R. Batiza, R. Haymon, A. Barone, W.B.F. Rzan, T. Smith, T. Simkin, and M.A. Luckman, Geochemical and structural studies of the Lamont Seamounts: Seamounts as indicators of mantle processes, *Earth Planet. Sci. Lett.*, *89*, 63-83, 1988.

Gautneb, H., and A. Gudmundsson, Effect of local and regional stress fields on sheet emplacement in west Iceland, *J. Volcanol. Geotherm. Res.*, *51*, 339-356, 1992.

Gautneb, H., A. Gudmundsson, and N. Oskarsson, Structure, petrochemistry and evolution of a sheet swarm in an Icelandic central volcano, *Geol. Mag.*, *126*, 659-673, 1989.

Gee, J., H. Staudigel, and J.H. Natland, Geology and petrology of Jasper Seamount, *J. Geophys. Res.*, *96*, 4083-4105, 1991.

Gee, M.J.R., The collapse of oceanic islands and the mechanics of long runout debris flows: Examples from the NW African margin, D. Phil. thesis, Univ. of Oxford, Oxford, England, 1999.

Grevemeyer, I., and W. Weigel, Increase of seismic velocities in upper oceanic crust: The "superfast" spreading East Pacific Rise at 14°14'S, *Geophys. Res. Lett.*, *24*, 214-220, 1997.

Grevemeyer, I., E. Flueh, C. Reichert, J. Bialas, D. Klaeschen, C. Kopp, and W. Weinrebe, Crustal and upper mantle structure of the Ninetyeast Ridge, Indian Ocean, *Eos Trans. AGU*, *79*(45), Fall Meet. Suppl., F871-F872, 1998.

Gudmundsson, A., Formation and development of normal-fault calderas and the initiation of large explosive eruptions, *Bull. Volcanol.*, *60*, 160-170, 1998a.

Gudmundsson, A., Magma chambers modeled as cavities explain the formation of rift zone central volcanoes and their eruption and intrusion statistics, *J. Geophys. Res.*, *103*, 7401-7412, 1998b.

Hammer, P.T.C., L.M. Dorman, J.A. Hildebrand, and B.D. Cornuelle, Jasper Seamount structure: Seafloor seismic refraction tomography, *J. Geophys. Res.*, *99*, 6731-6752, 1994.

Hammond, S.R., Offset caldera and crater collapse on Juan de Fuca ridge-flank volcanoes, *Bull. Volcanol.*, *58*, 617-627, 1997.

Head, J.W., and L. Wilson, Magma reservoirs and neutral buoyancy zones on Venus: Implications for the formation and evolution of volcanic landforms, *J. Geophys. Res.*, *97*, 3877-3903, 1992.

Herlihy, D.R., S.P. Matula, and C. Andreasen, Swath mapping data management within the National Oceanic and Atmospheric Administration, *Int. Hydrogr. Rev. Monoco*, *65*, 55-74, 1988.

Hill, D.P., and J.J. Zucca, Geophysical constraints on the structure of Kilauea and Mauna Loa volcanoes and some implications for seismomagmatic processes, in *Volcanism in Hawaii,* vol. 2, edited by R.W. Decker, T.L. Wright, and P.H. Stauffer, *U.S. Geol. Surv. Prof. Pap. 1350,* 903-917, 1987.

Hollister, C.D., F.F. Glenn, and P.F. Lonsdale, Morphology of seamounts in the western Pacific and Philippine Basin from multi-beam sonar data, *Earth Planet. Sci. Lett.*, *41*, 405-418, 1978.

Holmes, M.L., and H.P. Johnson, Upper crustal densities derived from sea-

floor gravity measurements: Northern Juan de Fuca Ridge, *Geophys. Res. Lett.*, *20*, 1871-1874, 1993.

Hooft, E.E., and R.S. Detrick, The role of density in the accumulation of basaltic melts at mid-ocean ridges, *Geophys. Res. Lett.*, *20*, 423-426, 1993.

Iverson, R.M., Can magma-injection and groundwater forces cause massive landslides on Hawaiian volcanoes?, *J. Volcanol. Geotherm. Res.*, *66*, 295-308, 1995.

Jordan, T.H., H.W. Menard, and D.K. Smith, Density and distribution of seamounts in the Eastern Pacific inferred from wide-beam sounding data, *J. Geophys. Res.*, *88*, 10,508-10,518, 1983.

Keating, B.H., Side-scan sonar images of submarine landslides on the flanks of atolls and guyots, *Mar. Geod.*, *21*, 129-145, 1998.

Keeley, C., W.B.F. Ryan, D. Caress, and W. Menke, RIDGE multibeam synthesis project, *RIDGE Events*, *5*(1), 5, 6, 18, 1994.

Klein, F.W., A linear gradient crustal model for south Hawaii, *Bull. Seismol. Soc. Am.*, *71*, 1503-1510, 1981.

Lacey, A., J.R. Ockendon, and D.L. Turcotte, On the geometrical form of volcanoes, *Earth Planet. Sci. Lett.*, *54*, 139-143, 1981.

Lipman, P.W., Subsidence of ash flow calderas: Relation to caldera size and magma-chamber geometry, *Bull. Volcanol.*, *59*, 198-218, 1997.

Lister, J.R., and R.C. Kerr, Fluid-mechanical models of crack propagation and their application to magma transport in dikes, *J. Geophys. Res.*, *96*, 10049-10077, 1991.

Lonsdale, P., Laccoliths(?) and small volcanoes on the flank of the East Pacific Rise, *Geology*, *11*, 706-709, 1983.

Lonsdale, P., A geomorphological reconnaissance of the submarine part of the East Rift Zone of Kilauea Volcano, Hawaii, *Bull. Volcanol.*, *51*, 123-144, 1989.

Lonsdale, P., and F.N. Spiess, A pair of young cratered volcanoes on the East Pacific Rise, *J. Geol.*, *87*, 157-173, 1979.

Lopez, D.L., and S.N. Williams, Catastrophic volcano collapse: Relation to hydrothermal alteration, *Science*, *260*, 1794-1796, 1993.

Macdonald, K.C., et al., The East Pacific Rise and its flanks, 8-18 N: History of segmentation, propagation and spreading direction based on SeaMARC II and SeaBeam studies, *Mar. Geophys. Res.*, *14*, 299-344, 1992.

MacPherson, G.J., The Snow Mountain volcanic complex: An on-land seamount in the Franciscan Terrain, California, *J. Geol.*, *91*, 73-92, 1983.

Masson, D.G., Catastrophic collapse of the volcanic island of Hierro 15 ka ago and the history of landslides in the Canary Islands, *Geology*, *24*, 231-234, 1996.

Masson, D.G., A.B. Watts, and the CD 108 Scientific Party, New sonar evidence for large-scale slope failures on the flanks of the Canary Islands, *Eos Trans. AGU*, *79*(17), Spring Meet. Suppl., S339, 1998.

McBirney, A.R., and H. Williams, Geology and petrology of the Galapagos Islands, *Mem. Geol. Soc. Am.*, *118*, 1969.

Mitchell, N.C., Characterising the irregular coastlines of volcanic ocean islands, *Geomorphology*, *23*, 1-14, 1998.

Mitchell, N.C., M.A. Tivey, and P. Gente, Slopes of mid-ocean ridge fault scarps from submersible observations, *Earth Planet. Sci. Lett.*, *in press*, 2000.

Moore, J.G., and W.W. Chadwick, Offshore geology of Mauna Loa and adjacent areas, Hawaii, in *Mauna Loa Revealed: Structure, Composition, History and Hazards*, Geophys. Monogr. Ser., vol. 92, edited by J. M. Rhodes and J. P. Lockwood, pp. 21-44, AGU, Washington, D. C., 1995.

Moore, J.G., D.A. Clague, R.T. Holcomb, P.W. Lipman, W.R. Normark, and M.E. Torresan, Prodigious submarine landslides on the Hawaiian Ridge, *J. Geophys. Res.*, *94*, 17,465-17,484, 1989.

Moore, J.G., W.R. Normark, and R.T. Holcomb, Giant Hawaiian landslides, *Annu. Rev. Earth Planet. Sci.*, *22*, 119-144, 1994.

Mouginis-Mark, P.J., S.K. Rowland, and H. Garbeil, Slopes of western Galapagos volcanoes from airborne interferometric radar, *Geophys. Res. Lett.*, *23*, 3767-3770, 1996.

Muller, R.D., W.R. Roest, J.-Y. Roger, L.M. Gahagan, and J.G. Sclater, Digital isochrons of the world's ocean floor, *J. Geophys. Res.*, *102*, 3211-3214, 1997.

Naumann, I., and D. Geist, Physical volcanology and structural development of Cerro Azul Volcano, Isabela Island, Galapagos: Implications for the development of Galapagos-type shield volcanoes, *Bull. Volcanol.*, *61*, 497-514, 2000.

Nercessian, A., A. Hirn, J.-C. Lepine, and M. Sapin, Internal structure of Piton de la Fournaise volcano from seismic wave propagation and earthquake distribution, *J. Volcanol. Geotherm. Res.*, *70*, 123-143, 1996.

Peirce, C., and P.J. Barton, Crustal structure of the Madeira-Tore Rise, eastern North Atlantic: Results of a DOBS wide-angle and normal incidence seismic experiment in the Josephine Seamount region, *Geophys. J. Int.*, *106*, 357-378, 1991.

Phipps Morgan, J., and Y.J. Chen, The genesis of oceanic crust: Magma injection, hydrothermal circulation, and crustal flow, *J. Geophys. Res.*, *98*, 6283-6297, 1993.

Purdy, G.M., L.S.L. Kong, G.L. Christeson, and S.C. Solomon, Relationship between spreading rate and the seismic structure of mid-ocean ridges, *Nature*, *355*, 815-817, 1992.

Rappaport, Y., D.F. Naar, C.C. Barton, Z.J. Liu, and R.N. Hey, Morphology and distribution of seamounts surrounding Easter Island, *J. Geophys. Res.*, *102*, 24713-24728, 1997.

Richey, J.E., *Scotland: The Tertiary Volcanic Districts,* 3rd ed., 120 pp., Gt. Brit. Geol. Surv., Regional Geology Handbook, 1961.

Roche, O., T.H. Druitt, and O. Merle, Experimental study of caldera formation, *J. Geophys. Res.*, *105*, 395-416, 2000.

Rubin, A.M., and D.D. Pollard, Origins of blade-like dikes in volcanic rift zones, in *Volcanism in Hawaii*, vol. 2, edited by R.W. Decker, T.L. Wright and P.H. Stauffer, *U.S. Geol. Surv. Prof. Pap.*, *1350*, 1449-1470, 1987.

Ryan, M.P., Neutral buoyancy and the mechanical evolution of magmatic systems, in *Magmatic Processes: Physiochemical Principles,* edited by B.O. Mysen, *Spec. Publ. Geochem. Soc. 1*, 259-287, 1987.

Scheirer, D.S., and K.C. Macdonald, Near-axis seamounts on the flanks of the East Pacific Rise, 8°N to 17°N, *J. Geophys. Res.*, *100*, 2239-2259, 1995.

Scheirer, D.S., K.C. Macdonald, D.W. Forsyth, S.P. Miller, D.J. Wright, M.-H. Cormier, and C.M. Weiland, A map series of the southern East Pacific Rise and its flanks 15°S to 19°S, *Mar. Geophys. Res.*, *18*, 1-12, 1996.

Schirnick, C., P. van den Bogaard, and H.-U. Schmincke, Cone sheet formation and intrusive growth of an oceanic island--The Miocene Tejeda complex on Gran Canaria (Canary Islands), *Geology*, *27*, 207-210, 1999.

Searle, R.C., Submarine central volcanoes on the Nazca plate: high-resolution sonar observations, *Mar. Geol.*, *53*, 77-102, 1983.

Simkin, T., Origin of some flat-topped volcanoes and guyots, *Mem. Geol. Soc. Am.*, *132*, 183-193, 1972.

Smith, D.K., Shape analysis of Pacific seamounts, *Earth Planet. Sci. Lett.*, *90*, 457-466, 1988.

Smith, D.K., Comparison of the shapes and sizes of seafloor volcanoes on Earth and "pancake" domes on Venus, *J. Volcanol. Geotherm. Res.*, *73*, 47-64, 1996.

Smith, D.K., and J.R. Cann, The role of seamount volcanism in crustal construction at the Mid-Atlantic Ridge (24°-30°N), *J. Geophys. Res.*, *97*, 1645-1658, 1992.

Smith, D.K., and T.H. Jordan, Seamount statistics in the Pacific Ocean, *J. Geophys. Res.*, *93*, 2899-2918, 1988.

Smith, T.L., and R. Batiza, New field and laboratory evidence for the origin of hyaloclastite, *Bull. Volcanol.*, *51*, 96-114, 1989.

Smoot, N.C., The Marcus-Wake seamounts and guyots as paleo-fracture indicators and their relation to the Dutton Ridge, *Mar. Geol.*, *88*, 117-131, 1989.

Staudigel, H., and H.U. Schmincke, The Pliocene seamount series of La Palma/Canary Island, *J. Geophys. Res.*, *89*, 11,195-11,215, 1984.

Stolper, E., and D. Walker, Melt density and the average composition of basalt, *Contrib. Mineral. Petrol.*, *74*, 7-12, 1980.

Sturgul, J.R., and Z. Grinshpan, Finite-element model of a mountain massif, *Geology*, *4*, 439-442, 1976.

Swift, S.A., H. Hoskins, and R.A. Stephen, Vertical seismic profile into upper oceanic crust in Hole 504B, *Proc. Ocean Drill. Program, Sci. Results*, 339-347, 1996.

Tucholke, B.E., W.K. Stewart, and M.C. Kleinrock, Long-term denudation of ocean crust in the central North Atlantic Ocean, *Geology*, *25*, 171-174, 1997.

Vera, E.E., J.C. Mutter, P. Buhl, J.A. Orcutt, A.J. Harding, M.E. Kappus, R.S. Detrick, and T.M. Brocher, The structure of 0- to 0.2-m.y.-old oceanic crust at 9°N on the East Pacific Rise from expanded spread profiles, *J. Geophys. Res.*, *95*, 15,529-15,556, 1990.

Vogt, P.R., Volcano height and plate thickness, *Earth Planet. Sci. Lett.*, *23*, 337-348, 1974.

Vogt, P.R., and N.C. Smoot, The Geisha Guyots: Multi-beam bathymetry

and morphometric interpretation, *J. Geophys. Res.*, *89*, 11,085-11,107, 1984.

Walker, G.P.L., Downsag calderas, ring faults, caldera sizes, and incremental caldera growth, *J. Geophys. Res.*, *89*, 8407-8416, 1984.

Walker, G.P.L., Gravitational (density) controls on volcanism, magma chambers and intrusions, *Aust. J. Earth Sci.*, *36*, 149-165, 1989.

Walsh, J.B., The effect of cracks on the compressibility of rocks, *J. Geophys. Res.*, *70*, 381-389, 1965.

Watts, A.B., J.H. Bodine, and N.M. Ribe, Observations of flexure and the geological evolution of the Pacific Ocean basin, *Nature*, *283*, 532-537, 1980.

Watts, A.B., C. Peirce, J. Collier, R. Dalwood, J.P. Canales, and T.J. Henstock, A seismic study of lithospheric flexure in the vicinity of Tenerife, Canary Islands, *Earth Planet. Sci. Lett.*, *146*, 431-447, 1997.

Weigel, W., and I. Grevemeyer, The Great Meteor Seamount: Seismic structure of a submerged intraplate volcano, *J. Geodyn.*, *28*, 27-40, 1999.

Wessel, P., and W.H.F. Smith, Free software helps map and display data, *Eos Trans. AGU*, *72*, 441, 445-446, 1991.

Wilkens, R.H., G.J. Fryer, and J. Karsten, Evolution of porosity and seismic structure of upper oceanic crust: Importance of aspect ratios, *J. Geophys. Res.*, *96*, 17,981-17,995, 1991.

Williams, H., and A.R. McBirney, *Volcanology*, 397pp., W. H. Freeman, New York, 1979.

Wilson, L., J.W. Head, and E.A. Parfitt, The relationship between the height of a volcano and the depth to its magma source zone: A critical reexamination, *Geophys. Res. Lett.*, *19*, 1395-1398, 1992.

Winterer, E.L., R. van Waasbergen, J. Mammerickx, and S. Stuart, Karst morphology and diagenesis of the top of Albian limestone platforms, Mid-Pacific Mountains, *Proc. Ocean Drill. Program, Sci. Results, 143*, 433-470, 1995.

Wyss, M., Hawaiian rifts and recent Icelandic volcanism: Expressions of plume generated radial stress fields, *J. Geophys.*, *19*, 19-22, 1980.

Zindler, A., H. Staudigel, and R. Batiza, Isotope and trace element geochemistry of young Pacific seamounts: Implications for the scale of upper mantle heterogeneity, *Earth Planet. Sci. Lett.*, *70*, 175-195, 1984.

N. C. Mitchell, Department of Earth Sciences, Cardiff University, P. O. Box 914, Cardiff CF10 3YE, Wales, U.K. (MitchellNC@cardiff.ac.uk)

(Received December 1, 1999; revised May 31, 2000;
accepted July 11, 2000.)